โครงสร้างและสมบัติเทอร์โมอิเล็กทริกของสารประกอบแลนทานัม
โคบอลต์ออกไซด์ที่มีการแทนที่แบบคู่ด้วยสตรอนเทียม
และแมกนีเซียม ณ อุณหภูมิห้อง

นางสาวอารีรัตน์ เจียมประเสริฐบุญ

วิทยานิพนธ์นี้เป็นส่วนหนึ่งของการศึกษาตามหลักสูตรปริญญาวิทยาศาสตรมหาบัณฑิต
สาขาวิชาเคมี
มหาวิทยาลัยเทคโนโลยีสุรนารี
ปีการศึกษา 2556

STRUCTURE AND THERMOELECTRIC PROPERTIES

OF Sr AND Mg DOUBLE-SUBSTITUTED LaCoO$_3$

AT ROOM TEMPERATURE

Arreerat Jiamprasertboon

A Thesis Submitted in Partial Fulfillment of the Requirements for the

Degree of Master of Science in Chemistry

Suranaree University of Technology

Academic Year 2013

STRUCTURE AND THERMOELECTRIC PROPERTIES OF

Sr AND Mg DOUBLE-SUBSTITUTED LaCoO$_3$

AT ROOM TEMPERATURE

Suranaree University of Technology has approved this thesis submitted in partial fulfillment of the requirements for a Master's Degree.

Thesis Examining Committee

_____

(Assoc. Prof. Dr. Jatuporn Wittayakun)

Chairperson

_____

(Dr. Theeranun Siritanon)

Member (Thesis Advisor)

_____

(Asst. Prof. Dr. Sanchai Prayoonpokarach)

Member

_____

(Asst. Prof. Dr. Rapee Gosalawit-Utke)

Member

_____   _____

(Prof. Dr. Sukit Limpijumnong)   (Assoc. Prof. Dr. Prapun Manyum)

Vice Rector for Academic Affairs   Dean of Institute of Science

and Innovation

อารีรัตน์ เจียมประเสริฐบุญ : โครงสร้างและสมบัติเทอร์โมอิเล็กทริกของสารประกอบ
แลนทานัมโคบอลต์ออกไซด์ที่มีการแทนที่แบบคู่ด้วยสตรอนเทียมและแมกนีเซียม ณ
อุณหภูมิห้อง (STRUCTURE AND THERMOELECRIC PROPERTIES OF Sr AND Mg
DOUBLE-SUBSTITUTED LaCoO$_3$ AT ROOM TEMPERATURE) อาจารย์ที่ปรึกษา :
อาจารย์ ดร.ธีรนันท์ ศิริตานนท์, 74 หน้า.

กลยุทธ์ในการปรับปรุงสมบัติเทอร์โมอิเล็กทริกของสารประกอบแลนทานัมโคบอลต์
ออกไซด์ (LaCoO$_3$) โดยการแทนที่แบบคู่ด้วยสตรอนเทียม (Sr) และ แมกนีเซียม (Mg) ใน
สารประกอบ La$_{1-x}$Sr$_x$Co$_{1-x}$Mg$_x$O$_3$ (เมื่อ x = 0, 0.025, 0.05, 0.1) ได้ถูกนำเสนอ ผลของการแทนที่
ของสตรอนเทียมหรือแมกนีเซียมได้ถูกศึกษาอย่างอิสระเช่นกันดังสารประกอบ La$_{1-x}$Sr$_x$CoO$_3$ และ
LaCo$_{1-x}$Mg$_x$O$_3$ (เมื่อ x = 0, 0.02, 0.05, 0.1, 0.2) สารตัวอย่างทั้งหมดถูกสังเคราะห์ด้วยวิธีซิเตรต
โซล-เจล การแทนที่แลนทานัม (La) ด้วยสตรอนเทียมในปริมาณเล็กน้อยเพิ่มค่าความสามารถใน
การนำไฟฟ้าแต่ลดค่าสัมประสิทธิ์ซีเบค แต่การลดลงของค่าสัมประสิทธิ์ซีเบคจะลดลงเมื่อ
สารประกอบถูกแทนที่ด้วยแมกนีเซียมในตำแหน่งของโคบอลต์ (Co) การแทนที่แบบคู่ของ
สตรอนเทียมและแมกนีเซียมส่งผลให้สารมีสมบัติเทอร์โมอิเล็กทริกดีขึ้นโดยที่ทั้งค่าความสามารถ
ในการนำไฟฟ้าและค่าสัมประสิทธิ์ซีเบคเพิ่มขึ้นในขณะที่ค่าความสามารถในการนำความร้อน
ลดลง ด้วยกลยุทธ์นี้ ตัวอย่างที่มีการแทนที่แบบคู่ในปริมาณเพียงเล็กน้อย ได้แก่
La$_{0.975}$Sr$_{0.025}$Co$_{0.0975}$Mg$_{0.025}$O$_3$ มีค่า ZT เท่ากับ 0.047 ณ อุณหภูมิห้อง

สาขาวิชาเคมี   ลายมือชื่อนักศึกษา_____

ปีการศึกษา 2556   ลายมือชื่ออาจารย์ที่ปรึกษา_____

ARREERAT JIAMPRASERTBOON : STRUCTURE AND THERMOELECRIC PROPERTIES OF Sr AND Mg DOUBLE-SUBSTITUTED $LaCoO_3$ AT ROOM TEMPERATURE. THESIS ADVISOR : THEERANUN SIRITANON, Ph.D. 74 PP.

THERMOELECTRICS/ELECTRICAL PROPERTIES/OXIDES/ CITRATE SOL-GEL METHOD

A strategy to improve the thermoelectric properties of $LaCoO_3$ by the double substitution of Sr and Mg in $La_{1-x}Sr_xCo_{1-x}Mg_xO_3$ (x = 0, 0.025, 0.05, 0.1) is presented. Effects of individual Sr or Mg substitution were also investigated separately in the series of $La_{1-x}Sr_xCoO_3$ and $LaCo_{1-x}Mg_xO_3$ (x = 0, 0.02, 0.05, 0.1, 0.2). All samples were successfully synthesized by the citrate sol-gel method. Replacing La by a small amount of Sr increases electronic conductivity but decreases the Seebeck coefficient; the decrease in the Seebeck coefficient is reduced when Mg is simultaneously substituted for Co. The employment of both Sr and Mg substitutions benefits the enhancement in thermoelectric efficiency since both electrical conductivity and Seebeck coefficient are enhanced while thermal conductivity is suppressed. With this strategy, the sample with a small amount of double substitution, $La_{0.975}Sr_{0.025}Co_{0.0975}Mg_{0.025}O_3$, exhibits a ZT of 0.047 at room temperature.

School of Chemistry   Student's Signature _____

Academic Year 2013   Advisor's Signature _____

ACKNOWLEDGEMENTS

I am so glad that all parts of this thesis have been fulfilled. Everything I have studied within this thesis has been greatly supported by my advisor, Dr. Theeranun Siritanon. She is a wonderful advisor as she is intelligent, reasonable, positive, and kind. She is an expert in the field of solid state chemistry, materials chemistry, as well as general chemistry. The way she guided me to approach these kinds of knowledge is also very interesting. Moreover, I am so grateful for her patience to advise and encourage me throughout the project. Dr. Theeranun thought reasonably and positively in every conversation we have had. This indirectly taught me to be a reasonable person who thinks positively. In addition, her kindness was the most important factor in assisting me to pass through every problem. Furthermore, she is a real teacher who opens the door of opportunity for a student when she can. I really appreciate everything she has given me. For the above reasons, it is a great pleasure being one of her students.

I would like to acknowledge the committee including Assoc. Prof. Dr. Jatuporn Wittayakun, Asst. Prof. Dr. Sanchai Prayoonpokarach, and Asst. Prof. Dr. Rapee Gosalawit-Utke. Their comments and suggestions were very useful for my thesis.

I also would like to thank Prof. Zenji Hiroi for giving me the opportunity to work in his laboratory. Thermoelectric properties measurement in this work was supported by the Institute for Solid State Physics (ISSP), The University of Tokyo. I am grateful to Dr. Yoshihiko Okamoto for his assistance in the measurements. I am honored to have had the chance to interact and learn with Prof. Zenji Hiroi and his

research group members. I also enjoyed the great opportunity of taking an educational tour at the Institute for Chemical Research and the Solid State Physics and Chemistry Laboratory, Kyoto University. Through his kindness and opened mind, I gained a great number of research and life experiences.

I am thankful to Prof. Mas Subramanian for providing his laboratory at the Department of Chemistry, Oregon State University, USA, where I learned the experimental techniques necessary to the field of Solid State Chemistry. It has been a special experience to discuss and study with him and his research group members. I would like to thank Dr. Jun Li for her valuable discussions and assistance in my experiments.

All experiments in this work could not have been done without the help and support from the people of Suranaree University of Technology: the research group member (Nararat Yong), colleagues in the School of Chemistry, colleagues in the School of Physics, and office staff in the Center for Scientific and Technological Equipment. Also, many thanks for the Center for Scientific and Technological Equipment (CSTE) and Advanced Materials Physics Laboratory (AMP) for providing facilities for my research.

Importantly, I would like to acknowledge the Thai Government for their support through the Development and Promotion of Science and Technology Talent Project (DPST) for financial supports.

Last but not least, I would like to express my deepest appreciation to my family: my father, mother, and sisters for their endless love, encouragement and support.

<div style="text-align: right;">Arreerat Jiamprasertboon</div>

CONTENTS

CONTENTS (Continued)

CONTENTS (Continued)

LIST OF TABLES

LIST OF FIGURES

LIST OF FIGURES (Continued)

LIST OF FIGURES (Continued)

LIST OF FIGURES (Continued)

LIST OF ABBREVIATIONS AND SYMBOLS

θ	angle
n	charge carrier concentration
10Dq	crystal field splitting energy
e	electric charge
μ	electron mobility
σ	electrical conductivity
ρ	electrical resistivity
κ_E	electronic thermal conductivity
r	ionic radius
κ_L	lattice thermal conductivity
Ω	Ohm
κ	thermal conductivity
κ_T	total thermal conductivity
t	tolerance factor
λ	wavelength
AC	alternating current
C	Coulomb
d	spacing between the planes in an atomic
DSP	digital signal processor
E_a	activation energy

LIST OF ABBREVIATIONS (Continued)

EDS	Energy Dispersive X-ray Spectroscopy
FESEM	Field Emission Scanning Electron Microscope
FT-IR	Fourier Transform Infrared Spectrometer
g_3 (g_4)	number of spin states for Co^{3+} (Co^{4+})
HS	high-spin state
I	current
IS	intermediate-spin state
J	Joule
K	Kelvin
k_B	Boltzmann constant
L	Lorenz factor
LS	low-spin state
n	integer
PPMS	Physical Properties Measurement System
s	second
S	Seebeck coefficient
STA	Simultaneous Thermal Analyzer
T	temperature
TG/DTA	Thermogravimetry/Differential Thermal Analysis
TTO	Thermal Transport Option
V	Volt
W	watt

LIST OF ABBREVIATIONS (Continued)

XRD   X-ray Diffraction

ZT   figure of merit
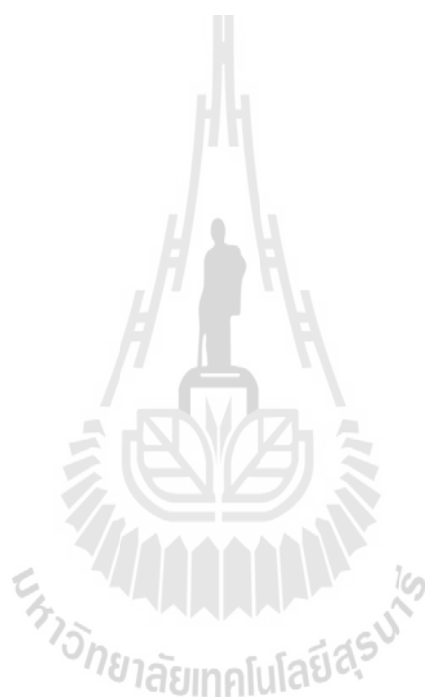
CHAPTER I

INTRODUCTION

1.1 Introduction

Concerning energy crisis and environmental problems, the fossil fuel consumption has unfortunately increased together with the release of toxic gases such as greenhouse gases. Moreover, the industrial system can utilize only less than 50% of fuels, while the remaining is exhausted to air as a waste heat (Ohta *et al.*, 2008). Hence, it is beneficial to increase the efficiency of the energy consumption. Among the alternative energy technologies, thermoelectric energy conversion is promising due to its ability to recycle wasted heat into electricity. Its properties allow applications on both electrical power generation and various electronic cooling devices (Elsheikh *et al*., 2014).

The performance of thermoelectric materials is defined by the figure of merit, ZT; $ZT = (S^2\sigma)T/\kappa$, when S, σ, and κ are Seebeck coefficient, electrical conductivity, and thermal conductivity, respectively. In general, a value of $ZT \geq 1$ is required for practical uses. The materials that show the best thermoelectric properties are alloys such as Bi_2Te_3, PbTe, and $Si_{1-x}Ge_x$ (Mahan, 1998; Sales *et al*., 1996; Yamashita *et al*., 2003). However, their uses are limited at low temperature as they have low stability and high toxicity. In contrast, oxides are more environmental friendly and have excellent thermal and chemical stability. As they are chemically stable at high temperature in air, thermoelectric oxides are expected to be used in much wider

(Cheng *et al*., 2006)

Oxides have advantage over classical heavy-element based compounds because they have higher thermal stability and ability to resist the oxidation reaction which can result in the release toxic substances (He *et al*., 2011). Cobalt oxides are interesting in this field as they were reported to have good thermoelectric properties, for example, $NaCo_2O_4$ has large Seebeck coefficient of 100 μVK^{-1} at 300 K (Terasaki *et al*., 1997), $Ca_2Co_2O_5$ has ZT of about 1.2-2.7 at $\geq$ 873 K (Funahashi *et al*., 2000), and $Bi_2Sr_2Co_2O_y$ has ZT $\geq$ 1.1 at 973 K (Funahashi and Shikano, 2002). Nevertheless, their layered structures lead to anisotropic properties that might cause difficulties in fabrication processes (Koumoto *et al*., 2006). As a consequence, a perovskite-type structure of metal oxides such as $LaCoO_3$ (Señarís-Rodríguez and Goodenough, 1995), $SrTiO_3$ (Ohta *et al*., 2005), and $Ca_{1-x}M_xMnO_3$ (when M = Tb, Ho, Y) (Kobayashi *et al*., 1991) may be the potential candidate for thermoelectric applications.

$LaCoO_3$-based oxides have received interest as thermoelectric materials. The important finding is the discovery of its high Seebeck coefficient of about 600 μVK^{-1} at room temperature (Señarís-Rodríguez and Goodenough, 1995). This value is higher comparing to other well-known thermoelectric cobalt oxide-based materials; for example, Na_xCoO_2, $Ca_2Co_2O_5$, and $Bi_2Sr_2Co_2O_y$ have room-temperature Seebeck coefficient of about 100 μVK^{-1}, 125 μVK^{-1}, and 160 μVK^{-1}, respectively. At 300 K, these cobalt oxides show figure of merit ZT of 0.6 (Terasaki *et al*., 1997), 0.026 (Funahashi *et al*., 2000), and about 0.023 (Funahashi and Shikano, 2002), respectively. Vulchev *et al*. (2012) also reported high Seebeck coefficient of $LaCoO_3$ of about 600 μVK^{-1}; nevertheless, its ZT value was very low, approximately 0.015 at 300 K.

Furthermore, $LaCoO_3$ prepared by Iwasaki *et al*. (2008) showed similar Seebeck coefficient value of about 500 μVK^{-1} with very low ZT of 0.003 at room temperature. Despite the high Seebeck coefficient, ZT of $LaCoO_3$ is very low because of the low electrical conductivity (Weidenkaff *et al*., 2008). Therefore, electrical conductivity as well as thermal conductivity has to be optimized to improve the ZT.

Doping some cations at La or Co site to create various $LaCoO_3$-based oxides is a common strategy used for such improvement. Sr substitution for La is widely investigated since it was found that $La_{0.95}Sr_{0.05}CoO_3$ shows the outstanding ZT of 0.18 at 300 K (Androulakis *et al*., 2004). Sr substitution normally increases electrical conductivity; however, it always decreases Seebeck coefficient (Mandal *et al.*, 2005; Zhou *et al.*, 2006; Zhou *et al.*, 2008a; Zhou *et al.*, 2008b; Iwasaki *et al.*, 2008). Moreover, substitution with some cations such as Ba (Hejtmánek *et al.*, 2004; Mandal *et al.*, 2004), Ca (Weidenkaff *et al.*, 2008), and Ni (Li and Li, 2011; Robert *et al.*, 2008; Kozuka *et al.*, 2012; Vulchev *et al.*, 2012; Robert *et al.*, 2006; Robert *et al.*, 2007) shows similar effects. On the other hand, some cations such as Mg (Ramadass *et al.*, 1979; Hejtmánek *et al.*, 2008; Jirák *et al*., 2008), and Fe (Rao *et al*., 1975; Vulchev *et al*., 2012) show interesting effect as their substitutions maintains the high Seebeck coefficient while the electrical conductivity is enhanced in the case of Mg and slightly decreased in the case of Fe. Considering the denominator of ZT, thermal conductivity is the only one devisor. This factor can be suppressed by some strategies including substitutions with cations such as Rh (Li *et al*., 2010), Na, and Pb (He *et al*., 2006).

Yet the single substitution cannot improve all parameters at the same time because they are interrelated. One of the strategies to enhance thermoelectric

properties has recently been conducted by double substitution. In 2003, Suzuki *et al*. (2003) prepared Sr and Mn double-substituted $LaCoO_3$. $La_{0.8}Sr_{0.2}Co_{1-x}Mn_xO_3$ (x = 0, 0.05, 0.10) presents coexistent consequences of each dopant resulting in developed ZT although Sr and Mn work together to improve only two of three parameters. Moreover, Rodríguez *et al*. (2008) prepared $La_{0.8}Sr_{0.2}Co_{1-x}Mn_xO_3$ (x = 0, 0.02, 0.03, 0.05) and found that $La_{0.8}Sr_{0.2}Co_{0.95}Mn_{0.05}O_3$ has ZT of 0.12. Besides, Ni and Fe double substitution was investigated by Vulchev *et al*. (2012). With $LaCo_{1-x}(Ni_{0.5}Fe_{0.5})_xO_3$ formula, Ni plays an important role to heighten the electrical conductivity while Fe keeps Seebeck coefficient at high value. Furthermore, 20-50% double-substituted $LaCoO_3$ effectively suppresses thermal conductivity comparing to its parent compound. This work illustrates the success of simultaneous effect from each cation on amelioration for all parameters of thermoelectric properties. Therefore, numerous series of co-doping is interesting.

Herein, this study focuses on improving the thermoelectric performance of $LaCoO_3$-based oxides by double substitution of La and Co with Sr and Mg. The synergic effect of the two doping cations is expected to improve the material properties favorably. At the same time, the sol-gel method is employed for all sample preparations in order to control the microstructure of materials. This sample preparation method is expected to result in smaller particles which should lower thermal conductivity. TG/DTA and FT-IR were utilized to obtain the optimal condition of syntheses. Structural identification was mainly investigated by X-Ray diffraction. Refinement using Le Bail method provided structural details of lattice parameters. In addition, the influence of both single and double substitutions of Co and/or La as well as compositions on thermoelectric properties was evaluated in the

term of the figure of merit ZT at room temperature. A Quantum Design Physical Properties Measurement System (PPMS) was employed to obtain ZT by the simultaneous measurement of electrical resistivity (ρ), Seebeck coefficient (S), and thermal conductivity (κ).

1.2 References

Androulakis, J., Migiakis, P., and Giapintzakis, J. (2004). $La_{0.95}Sr_{0.05}CoO_3$: An efficient room-temperature thermoelectric oxide. **Appl. Phys. Lett.** 84: 1099-1101.

Cheng, J., Sui, Y., Fu, H., Lu, Z., Wei, B., Qian, Z., Miao, J., Liu, Z., Huang, X., Zhu, R., Wang, X., and Su, W. (2006). Fabrication and thermoelectric properties of highly textured $NaCo_2O_4$ ceramic. **J. Alloy. Compd.** 407: 299-303.

Elsheikha, M. H., Shnawah, D. A., Sabri, M. F. M., Said, S. B. M., Hassan, M. H., Bashir, M. B. A., and Mohamad, M. (2014). A review on thermoelectric renewable energy: principle parameters that affect their performance. **Renew. Sust. Energ. Rev.** 30: 337-355.

Funahashi, R., Matsubara, I., Ikuta, H., Takeuchi, T., Mizutani, U., and Sodeoka, S. (2000). An oxide single crystal with high thermoelectric performance in air. **Jpn. J. Appl. Phys.** 39: L1127-L1129.

Funahashi, R. and Shikano, M. (2002). $Bi_2Sr_2Co_2O_y$ whiskers with high thermoelectric figure of merit. **Appl. Phys. Lett.** 81: 1459-1461.

He, J., Liu. Y., and Funahashi, R. (2011). Oxide thermoelectrics: The challenges, progress, and outlook. **J. Mater. Res.** 26: 1762-1772

He, T., Chen, J., Calvarese, T. G., and Subramanian, M. A. (2006). Thermoelectric

properties of $La_{1-x}A_xCoO_3$ (A = Pb, Na). **Solid State Sci.** 8: 467-469.

Hejtmánek, J., Jirák, Z., Knižek, K., Maryško, K., Veverka, M., and Fujishiro, H. (2004). Magnetism, structure and transport of $Y_{1-x}Ca_xCoO_3$ and $La_{1-x}Ba_xCoO_3$. **J. Magn. Magn. Mater.** 272–276: e283-e284.

Hejtmánek, J., Jirák, Z., Knížek, K., Maryško, M., Veverka, M., and Autret, C. (2008). Valence and spin states in perovskites $LaCo_{0.95}M_{0.05}O_3$ (M = Mg, Ga,Ti). **J. Magn. Magn. Mater.** 320: e92-e95.

Iwasaki, K., Ito, T., Nagasaki, T., Arita, Y., Yoshino, M., and Matsui, T. (2008). Thermoelectric properties of polycrystalline $La_{1-x}Sr_xCoO_3$. **J. Solid State Chem.** 181: 3145-3150.

Jirák, Z., Hejtmánek, J., Knížek, K., and Veverka, M. (2008). Electrical resistivity and thermopower measurements of the hole- and electron-doped cobaltites $LnCoO_3$. **Phys. Rev. B.** 78: 014432.

Kobayashi, T., Takizawa, H., Endo, T., Sato, T., Shimada, M., Taguchi, H., and Nagao, M. (1991). Metal-insulator transition and thermoelectric properties in the system $(R_{1-x}Ca_x)Mn_{3-\delta}$, (R: Tb, Ho, Y). **J. Solid State Chem.** 92: 116-129.

Koumoto, K., Terasaki, I., and Funahashi, R., (2006). Complex oxide materials for potential thermoelectric applications. **Mater. Res. Bull.** 31: 206-210.

Kozuka, H., Ohbayashi, K., and Koumoto, K. (2012). $LaCo_{1-x}Ni_xO_3$ with improved electrical conductivity. **Inorg. Chem.** 51: 9259-9264.

Li, J., Smith, A. E., Kwong, K.-S., Powell, C., Sleight, A. W., and Subramanian, M. A. (2010). Lattice crossover and mixed valency in the $LaCo_{1-x}Rh_xO_3$ solid solution. **J. Solid State Chem.** 183: 1388-1393.

Li, F. and Li, J.-F. (2011). Effect of Ni substitution on electrical and thermoelectric properties of LaCoO$_3$ ceramics. **Ceram. Int.** 37: 105-110.

Mahan, G. D. (1998). Good thermoelectrics. **Solid State Phys.** 51: 81-157.

Mandal, P., Choudhury, P., Biswas, S. K., and Ghosh, B. (2004). Transport and magnetic properties of La$_{1-x}$Ba$_x$CoO$_3$. **Phys. Rev. B.** 70: 104407-1-104407-8.

Mandal, P., Choudhury, P., and Ghosh, B. (2005). Transport studies of metallic La$_{1-x}$A$_x$CoO$_3$ (A = Sr, Ba) ferromagnet. **Physica B.** 359-361: 1363-1365.

Ohta, S., Nomura, T., Ohta, H., and Koumoto, K. (2005) High-temperature carrier transport and thermoelectric properties of heavily La- or Nb-doped SrTiO$_3$ single crystals. **J. Appl. Phys.** 97: 034106-1-034106-4.

Ohta, H., Sugiura, K., and Koumoto, K., (2008). Recent progress in oxide thermoelectric materials: p-type Ca$_3$Co$_4$O$_9$ and n-type SrTiO$_3^-$. **Inorg. Chem.** 47: 8429-8436.

Ramadass, N., Gopalakrishnan, J., and Sastri, M. V. C. (1979). Studies on magnesium- and titanium-substituted LaCoO$_3$. **J. Less-Common. Met.** 65: 129-138.

Rao, C. N. R., Parkash, O. M., and Ganguly, P. (1975). Electronic and magnetic properties of LaNi$_{1-x}$Co$_x$O$_3$, LaCo$_{1-x}$Fe$_x$O$_3$, and LaNi$_{1-x}$Fe$_x$O$_3$. **J. Solid State Chem.** 15: 186-192.

Robert, R., Bocher, L., Trottmann, M., and Weidenkaff, A. (2006). Synthesis and high-temperature thermoelectric properties of Ni and Ti substituted LaCoO$_3$. **J. Solid State Chem.** 179: 3893-3899.

Robert, R., Bocher, L., Sipos, B., Döbeli, M., and Weidenkaff, A. (2007). Ni-doped cobaltates as potential materials for high temperature solar thermoelectric converters. **Prog. Solid State Ch.** 35: 447-455.

Robert, R., Aguirre, M. H., Bocher, L., Trottmann, M., Heiroth, S., Lippert, T., Döbeli, M., and Weidenkaff., A. (2008). Thermoelectric properties of $LaCo_{1-x}Ni_xO_3$ polycrystalline samples and epitaxial thin films. **Solid State Sci.** 10: 502-507.

Rodríguez, J. E., Cadavid, D., and Moreno, L. C. (2008). Thermoelectric figure of merit of LSCoO-Mn perovskites. **Microelectr. J.** 39: 1236-1238.

Sales, B. C., Mandrus, D., and Williams, R. K. (1996). Filled skutterudite antimonides: a new class of thermoelectric materials. **Science.** 272: 1325-1328.

Señarís-Rodríguez, M. A. and Goodenough, J. B. (1995). $LaCoO_3$ revisited. **J. Solid State Chem.** 116: 224-231.

Suzuki, K., Fujishiro, H., Kashiwada, Y., Fujine, Y., and Ikebe, M. (2003). Magnetic, electrical and thermal properties of $La_{0.80}Sr_{0.20}(Mn_yCo_{1-y})O_3$. **Physica B.** 329-333: 922-923.

Terasaki, I., Sasago, Y., and Uchinokura, K. (1997). Large thermoelectric power in $NaCo_2O_4$ single crystals. **Phys. Rev. B.** 56: R12685-R12687.

Vulchev, V., Vassilev, L., Harizanova, S., Khristov, M., Zhecheva, E., and Stoyanova, R. (2012). Improving of the thermoelectric efficiency of $LaCoO_3$ by double substitution with nickel and iron. **J. Phys. Chem. C.** 116: 13507-13515.

Weidenkaff, A., Robert, R., Aguirre, M., Bocher, L., Lippert, T., and Canulescu, S. (2008). Development of thermoelectric oxides for renewable energy conversion technologies. **Renew. Energ.** 33: 342-347.

Yamashita, O., Tomiyoshi, S., and Makita, K. (2003). Bismuth telluride compounds with high thermoelectric figures of merit. **J. Appl. Phys.** 93: 368-374.

Zhou, A. J., Zhu, T. J., and Zhao, X. B. (2006). Thermoelectric properties of perovskite-type oxide $La_{1-x}Sr_xCoO_3$ (x = 0, 0.1) prepared by solid state reactions. **Mater. Sci. Eng**. **B.** 128: 174-178.

Zhou, A. J., Zhu, T. J., and Zhao, X. B. (2008a). Thermoelectric properties of perovskite oxides $La_{1-x}Sr_xCoO_3$ prepared by polymerlized complex method. **J. Mater. Sci.** 43: 1520-1524.

Zhou, A. J., Zhu, T. J., Zhao, X. B., Chen, H. Y., and Müller, E. (2008b). Fabrication and thermoelectric properties of perovskite-type oxide $La_{1-x}Sr_xCoO_3$ (x = 0, 0.1). **J. Alloy. Compd.** 449: 105-108.
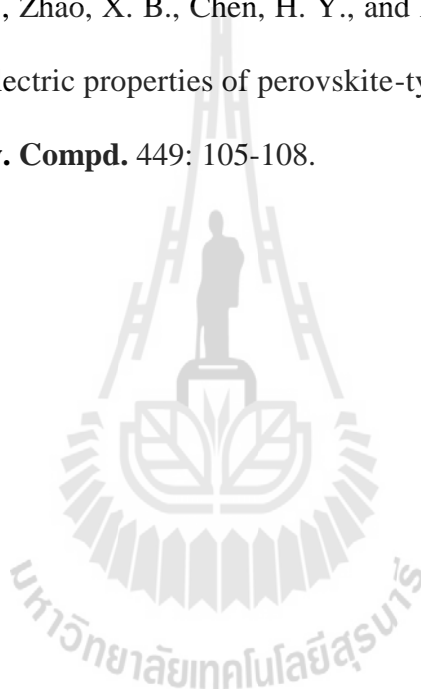
CHAPTER II

LITERATURE REVIEW

2.1 Thermoelectric materials

Thermoelectric materials exhibit the phenomenon of heat and electricity conversion. The phenomenon is based on two important effects, Seebeck (Seebeck, 1823) and Peltier effects (Peltier, 1834). The Seebeck effect, which is used in a power generation mode, is a development of voltage across the junction of two different materials held at different temperature (Figure 2.1a). On the other hand, the Peltier effect used in refrigeration mode involves a heat liberation or absorption when electrical current is applied to such junction (Figure 2.1b).
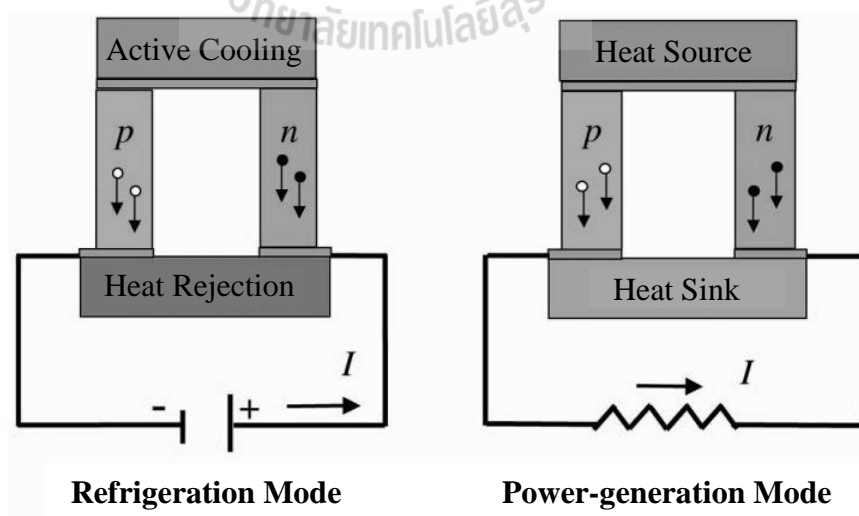
Figure 2.1 Diagram of a thermoelectric device made of n-type and p-type materials in

(a) a refrigeration or (b) a power-generation modes (Tritt and Subramanian, 2006).

The performance of a thermoelectric material is defined by the dimensionless figure of merit, ZT;

$$ZT = \frac{S^2 \sigma T}{\kappa} = \frac{S^2 T}{\rho \kappa} \tag{1}$$

where S is the Seebeck coefficient, σ is the electrical conductivity, ρ is the electrical resistivity, κ_T is the total thermal conductivity ($\kappa_T = \kappa_E + \kappa_L$; κ_E and κ_L are the electronic and the lattice contributions, respectively), and T is the absolute temperature. To maximize the ZT value, high S, high σ, and low κ are required (Tritt and Subramanian, 2006). These factors are closely related, such that charge carrier concentration has to be optimized (Weidenkaff *et al*., 2008). In general, a carrier density of materials in the range of heavily-doped semiconductors exhibits large ZT values as shown in Figure 2.2 (Snyder and Toberer, 2008).
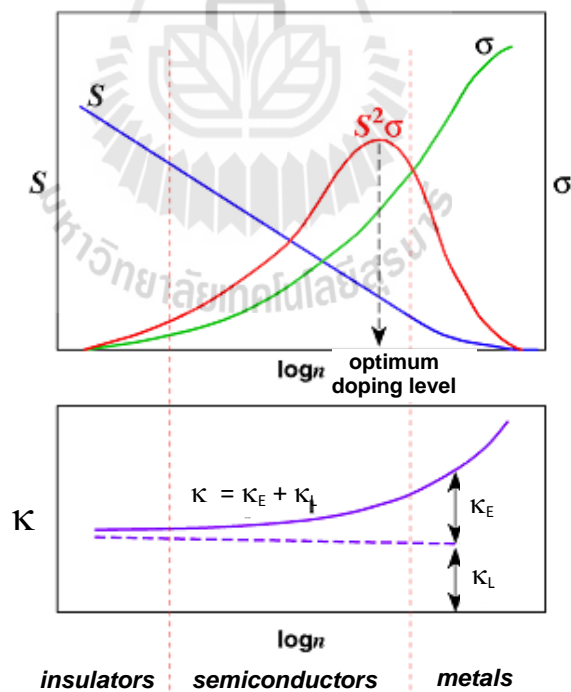
Figure 2.2 Transport properties as a function of a carrier concentration (Ohtaki, 2011).

Besides the high ZT value, the operating temperature of a system is also important for real applications. As shown in Figure 2.3, each material has different

operating temperature and the materials with wider ranges of operating temperatures have more potential for the real applications.

Environmental and beneficial issues have to be considered to develop suitable thermoelectric materials. Compounds such as alloys and chalcogenides have disadvantages because of their poor durability at raised temperature, low abundance, high cost of the comprising elements, and high toxicity. It is therefore necessary to explore new thermoelectric materials to overcome these shortcomings (Ohtaki, 2011).
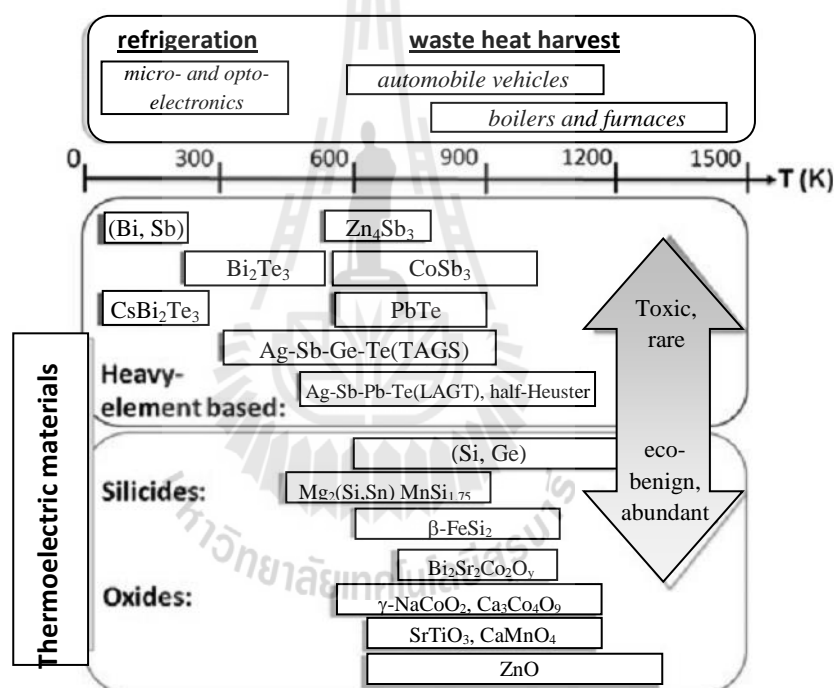
Figure 2.3 Diagrammatic comparisons of diverse thermoelectric materials for the applications as a function of the operating temperature, the abundance, and the toxicity (He *et al.*, 2011).

2.2 LaCoO₃-based thermoelectric oxides

This part discusses the structural details and related researches of the LaCoO₃-related systems.

2.2.1 Structure of LaCoO₃

LaCoO$_3$ structure is related to perovskite of general formula ABO$_3$, where A and B are two cations of very different sizes. In its cubic-symmetry structure (Figure 2.4a), B is the smaller cation surrounded by a six-fold coordination of oxygen forming an octahedron while A is the larger cation in a twelve-fold coordination. Each octahedral unit shares corners to form three-dimensional networks with B-O-B and O-B-O bond angles of 180° and 90°, respectively. The body-center position is occupied by the large A cation.

(a)　　　　　　　　　　(b)

● A
● B
• O
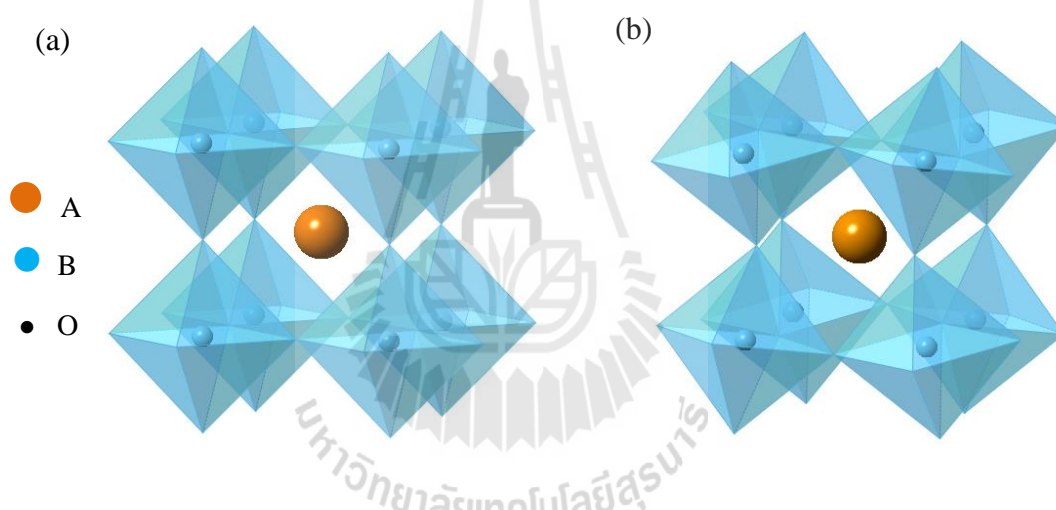
Figure 2.4 (a) a ABO$_3$ ideal perovskite structure and (b) a distorted perovskite structure.

Certain ratios of the ionic radii of A and B are required to stabilize the perovskite cubic structure. Otherwise, a distortion can lower a symmetry and a coordination number of cations might be reduced (Tejuca and Fierro, 1989). Actually, most perovskites are distorted from the ideal cubic structure by various factors such as the ionic size effects, the deviations from the ideal composition, and the Jahn-Teller effect (Johnsson and Lemmens, 2007). On the basis of the geometric considerations, Goldschmidt (1926) defined the tolerant limits of ionic radii through the tolerance

factor, $t = (r_A + r_O)/[\sqrt{2}(r_B + r_O)]$ where r_A, r_B, and r_O are the radii of A, B, and O ions, respectively. The ideal cubic perovskite $SrTiO_3$ with $r_{A(Sr)} = 1.44$ Å and $r_{B(Ti)} = 0.605$ Å, has $t = 1$ (Johnsson and Lemmens, 2007). In comparison, $LaCoO_3$ has similar B cation size ($r_{B(Co)} = 0.610$ Å) but smaller A cation ($r_{A(La)} = 1.36$ Å) which makes t become smaller than 1. As a result, the BO_6 octahedra tilt in order to fill a space and allow a distorted perovskite structure (Figure 2.4(b)). In fact, a cubic perovskite can be observed only for $0.81 \leq t \leq 1.11$ (Mitchell, 2002).

2.2.2 Thermoelectric properties of $LaCoO_3$-based oxides

$LaCoO_3$ is a p-type semiconducting material (Goodenough and Longo, 1970) in which its Seebeck coefficient (thermoelectric power or thermopower) is positive indicating that positive charge is the major carrier (Weidenkaff et al., 2008). The system of $LaCoO_3$ has been attractive in thermoelectric field because of its high Seebeck coefficient of about 600 μVK^{-1} at room temperature (Señarís-Rodríguez and Goodenough, 1995). However, the electrical resistivity is still high (Weidenkaff et al.,
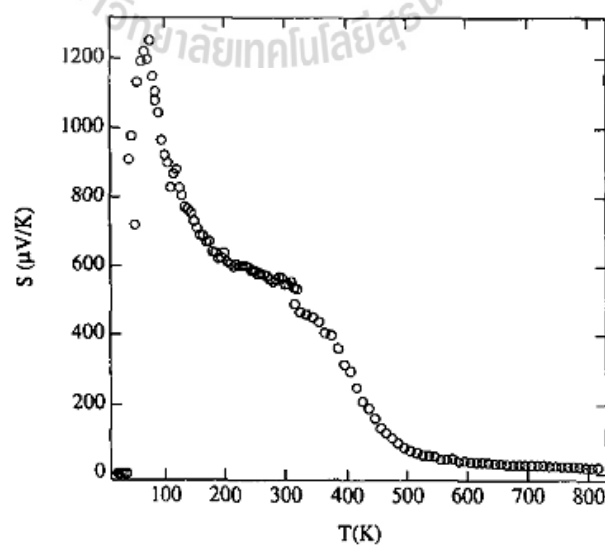
Figure 2.5 Temperature dependence of the Seebeck coefficient of $LaCoO_3$ (4.2 K< T<823 K) (Señarís-Rodríguez and Goodenough, 1995).

2008) which would lower the ZT value.

The amount of the charge transports in this system can be tuned by the level of Co-site and/or La-site substitution. Numerous strategies have been attempted to generate materials with high figure of merit, ZT, including increasing thermoelectric power and electrical conductivity as well as decreasing thermal conductivity.

2.2.2.1 Electrical conductivity improvement

Electrical conductivity (σ) or electrical resistivity (ρ) of materials relates to charge carrier concentration (n), electric charge (e), and electron mobility (μ) (Snyder and Toberer, 2008) by

$$\sigma = \frac{1}{\rho} = ne\mu \qquad (2)$$

Higher level of charge carrier concentration significantly increases electrical conductivity of oxides. In general, the charge carrier can be divided into two types; a hole and an electron which are dominant in p- and n-type semiconductors, respectively.

A p-type material can be produced by the substitution of parent cation by cations with lower valency which results in generation of positive hole carriers. In LaCoO$_3$ system, various cations have been utilized for the substitution of La- or Co-site; such as Sr^{2+}, Ba^{2+}, Ca^{2+}, Ni^{2+}, and Mg^{2+}. La substitution by Sr has received great attention since Androulakis $et\ al.$ (2004) discovered a high figure of merit, ZT, of 0.18 in La$_{0.95}$Sr$_{0.05}$CoO$_3$ at room temperature. In addition, Sr played an important role to almost completely suppress the resistivity of LaCoO$_3$. Then, the amount of 0.05-0.2 for Sr doping was studied by Zhou $et\ al.$ (2008b) from room temperature to 773 K; higher level of Sr doping resulted in higher electrical conductivity because of the higher carrier concentration. The replacement of La^{3+} by Sr^{2+} creates excess negative

charges in the lattice which are compensated either by oxidation of Co^{3+} to Co^{4+} and hence creates holes or by creation of oxygen vacancies to keep the electroneutrality of compounds (Mineshige *et al*., 1999). However, the Seebeck coefficients of all samples decreased dramatically in the temperature range below 550 K and remained constant up to 773 K. Yet the highest ZT of 0.046 was obtained with $La_{0.9}Sr_{0.1}CoO_3$. Moreover, thermoelectric properties of $La_{1-x}Sr_xCoO_3$ with x = 0.01-0.4 were investigated at 100-1000 K (Iwasaki *et al.*, 2008). It was found that the conductivity increased with increasing Sr content, on the contrary, the Seebeck coefficient was lowered (Figure 2.6-2.7). The same effects were reported in other substitutions both in La site such as Ba (Mandal *et al.*, 2004; Hejtmánek *et al.*, 2004), Ca (Weidenkaff *et al.*, 2008); and in Co substitution such as Ni (Kozuka *et al.*, 2012; Robert *et al.*, 2006; Robert *et al.*, 2007; Vulchev *et al.*, 2012). Although p-type substitution of $LaCoO_3$ plays an important role in enhancing electrical conductivity, it is usually accompanied by reduction of Seebeck coefficient.
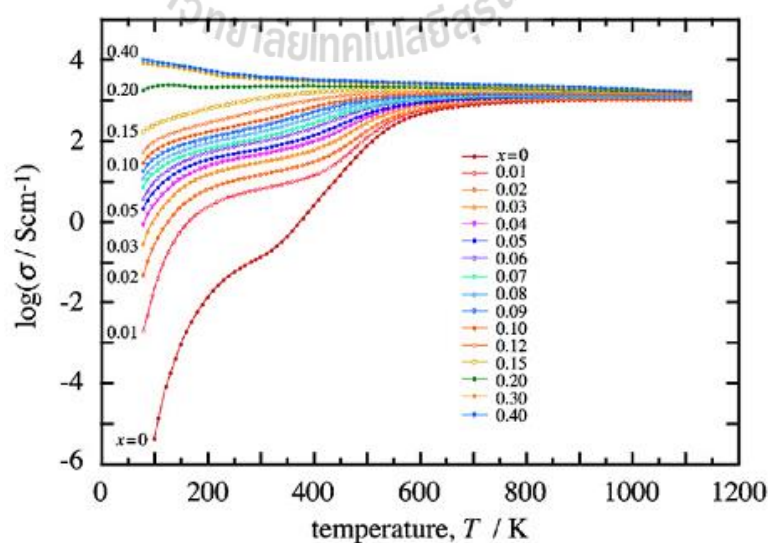
Figure 2.6 Temperature dependence of the electrical conductivity of $La_{1-x}Sr_xCoO_3$ (Iwasaki *et al.*, 2008).
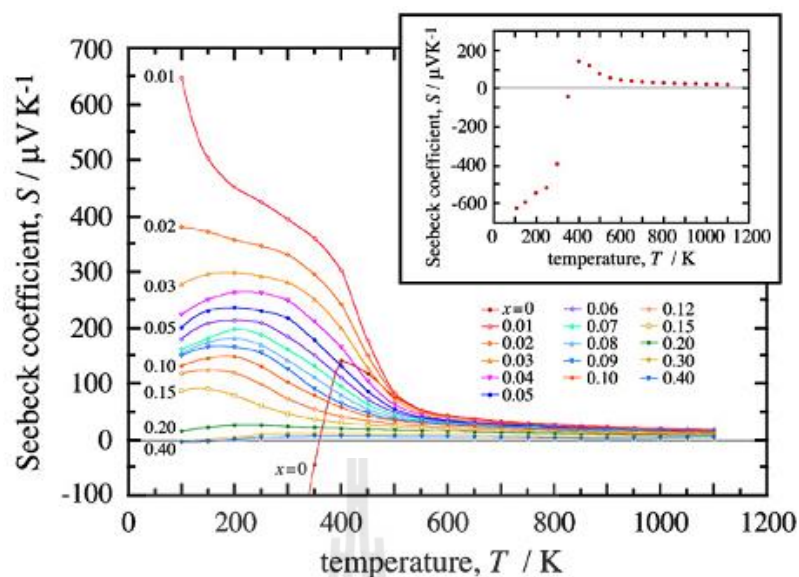
Figure 2.7 Temperature dependence of the Seebeck coefficient for $La_{1-x}Sr_xCoO_3$. The inset shows the Seebeck coefficient of non-doped $LaCoO_3$ (Iwasaki *et al.*, 2008).

An n-type material is generated by a higher valency cations replacement. Excess electrons are created as the carriers. Hébert *et al.* (2007) substituted Ce^{4+} for La-site in $LaCoO_3$. Co^{2+} was created by the reduction of Co^{3+} in order to balance total charges of the compound. The electrical resistivity of the Ce-substituted $LaCoO_3$ was lower than that of $LaCoO_3$ but still much higher than that of the Sr-doped $LaCoO_3$ (Figure 2.8).

The lower efficiency in n-type conduction attributes to the hopping mechanism of Co^{2+}/Co^{3+} system which is similar to 'spin-blockade' mechanism as previously proposed in $LnBaCo_2O_{5-\delta}$ (Maignan *et al*., 2004). The electron carriers in high spin (HS) state of Co^{2+} are impossible to interchange with low spin (LS) of Co^{3+} because of difference in e_g band energy level. Furthermore, Co^{2+} low spin configuration of $t_{2g}^6 e_g^1$ would be unstable. The hopping of one electron of HS Co^{2+} in the LS Co^{3+} matrix is thus forbidden (Hébert *et al*., 2007) (Figure 2.9).
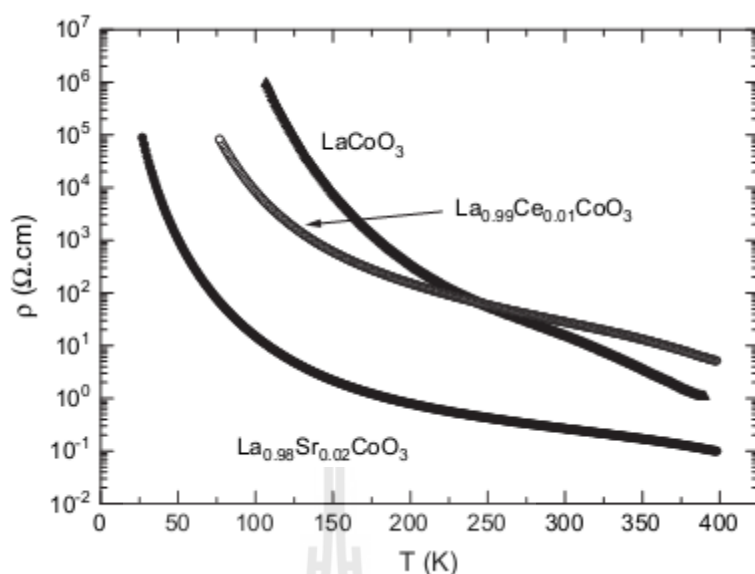
Figure 2.8 Temperature dependence of the electrical resistivity of LaCoO$_3$ comparing

with p-type La$_{0.98}$Sr$_{0.02}$CoO$_3$ and n-type La$_{0.99}$Ce$_{0.01}$CoO$_3$ (Hébert *et al*., 2007).
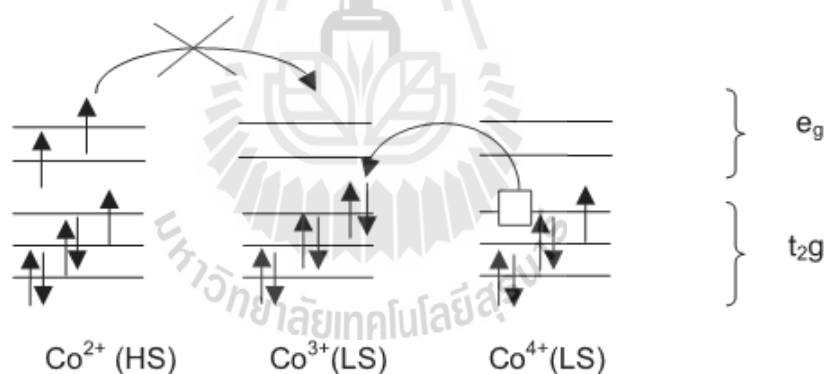
Figure 2.9 Schematic illustration of the transport mechanism in the e$_g$ band

(Co^{2+}/Co^{3+}) and in the t$_{2g}$ band (Co^{3+}/Co^{4+}) (Hébert *et al*., 2007).

On the contrary, Co^{3+}/Co^{4+} system in p-type LaCoO$_3$ greatly increases

conductivity because the carrier can easily hop between the same low-spin state

energy (Hébert *et al*., 2007).

Partially doping of a Co-site by Ti^{4+} was studied by Robert *et al.* (2006).

It was shown that resistivity increase with Ti content. This is in a good agreement with

the n-type transport mechanism as discussed above. In 2010, Robert *et al.* (2010) studied the wider range of a Ti substitution and found that the electrical resistivity varied with the amount of n-type dopant (Figure 2.10). Furthermore, the reported activation energy (E_a) of this system progressively increases with Ti content which is the reason of a high resistivity.
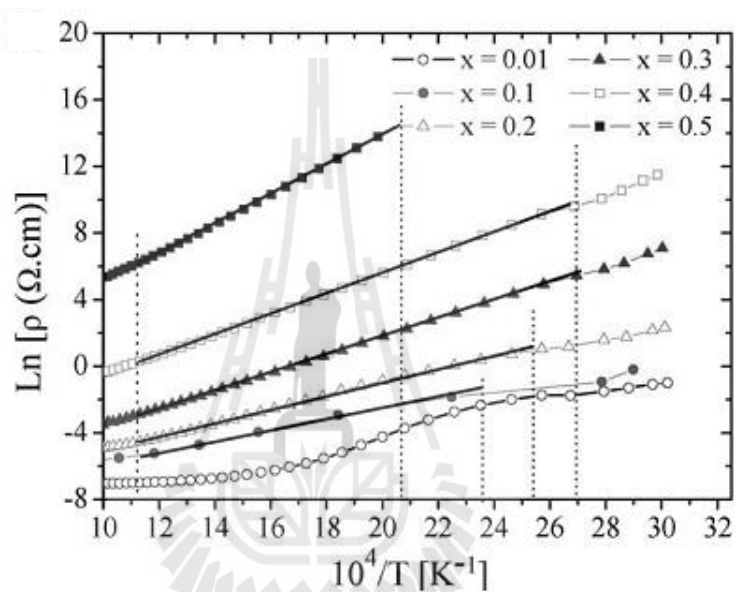
Figure 2.10 Plot of the electrical resistivity in the temperature range of 330 K<T<1273 K of $LaCo_{1-x}Ti_xO_3$ (x = 0.01-0.5) (Robert *et al.*, 2010).

As the thermoelectric device contains the couple consisting of p-type and n-type components, the improvement of both parts is importantly taken into account for an efficient gadget.

2.2.2.2 Seebeck coefficient improvement

The Seebeck coefficient of cobalt oxides was theoretically studied at a sufficient high temperature by formularizing the Heikes equation as expressed as

$$S = -\frac{k_B}{e}[\ln(\frac{g_3}{g_4})(\frac{x}{1-x})] \qquad (3)$$

where k_B is Boltzmann constant, e is electric charge, g_3 (g_4) is the number of spin states for Co^{3+} (Co^{4+}), and x is the concentration of Co^{4+} (Berggold *et al*., 2005; Chaikin and Beni, 1976; Koshibae *et al*., 2000).

Hund's rule coupling, crystal field splitting energy (10Dq), and temperature are related parameters that are used to determine the possible spin state, g_3 (g_4). The degeneracies of both Co^{3+} and Co^{4+} in low-spin state (LS), intermediate-spin state (IS), and high-spin state (HS) were proposed as shown in Figure 2.11. It was stated that the characteristic spin degeneracy and strong correlation of 3*d* electrons in cobalt oxides cause the large Seebeck coefficient. Moreover, the ratios of g_3/g_4 and x/1-x influence not only the magnitude but also the sign of S (Koshibe *et al*., 2000).
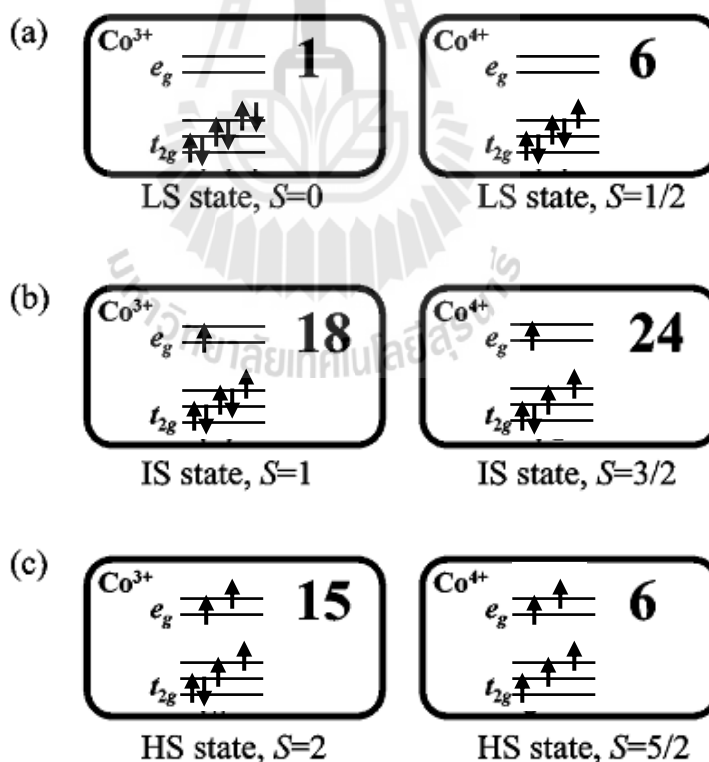
Figure 2.11 Schematic of spin degeneracy of 3*d* electron in Co^{3+} and Co^{4+} at (a) Low-spin state, (b) intermediate-spin state, (c) high-spin state, when degeneracy for each state is presented by the number in the frame and S is a spin multiplicity (modified

from Koshibae *et al.*, 2000).

Substitution with heterovalent cations, e.g., Sr-(Mandal *et al.*, 2005; Zhou *et al.*, 2006; Zhou *et al.*, 2008a; Zhou *et al.*, 2008b; Iwasaki *et al.*, 2008), Ba-(Hejtmánek *et al.*, 2004; Mandal *et al.*, 2004), Ca-(Weidenkaff *et al.*, 2008), and Ni-substitution (Li and Li, 2011; Robert *et al.*, 2008; Kozuka *et al.*, 2012; Vulchev *et al.*, 2012; Robert *et al.*, 2006; Robert *et al.*, 2007) usually increase electrical conductivity and decrease Seebeck coefficients. However, some of replacements such as Ti-(Robert *et al.*, 2010) and Rh-substitution (Li *et al.*, 2010) have opposite effects as they reduce electrical conductivity and raise Seebeck coefficient.

Among these results, Hejtmánek *et al.* (2008) found that the introduction of homovalent Ga^{3+} into Co-site results in similar resistivity and thermoelectric power behavior to $LaCoO_3$ which showed the Seebeck coefficient of 700 μVK^{-1} at 300 K (Figure 2.12). Heterovalent Mg-doping showed constant thermoelectric power in the same way as 0.02 Sr-doping from 100 to 300 K but with higher Seebeck coefficient of 400 μVK^{-1} at 300 K (Hejtmánek *et al.*, 2008). The Seebeck coefficient increases with Mg substitution but the values fall rapidly as the temperature increases (Ramadass *et al.*, 1979). Another interesting dopant which showed ability to maintain a high Seebeck coefficient is Fe. $LaCo_{1-x}Fe_xO_3$ (x = 0-0.5) can maintain Seebeck coefficient about 600 μVK^{-1} at room temperature (Vulchev *et al.*, 2012).

2.2.2.3 Thermal conductivity improvement

Electrical conductivity can be improved with various heterovalent substitutions, some of which can also maintain thermoelectric power. In addition, the ZT can be further maximized by minimizing thermal conductivity. This could be achieved by means of adjusting the crystallographic structure and increasing the

phonon scattering.

Total thermal conductivity (κ_T) comes from two sources: electronic (κ_E) and lattice (κ_L) part. κ_E is directly related to the electrical conductivity through the Wiedemann–Franz law:

$$\kappa_E = \sigma\text{LT} = ne\mu\text{LT} \tag{4}$$

where L is the Lorenz factor which is equal to 2.4×10^{-8} $J^2K^{-2}C^{-2}$ for free electrons.

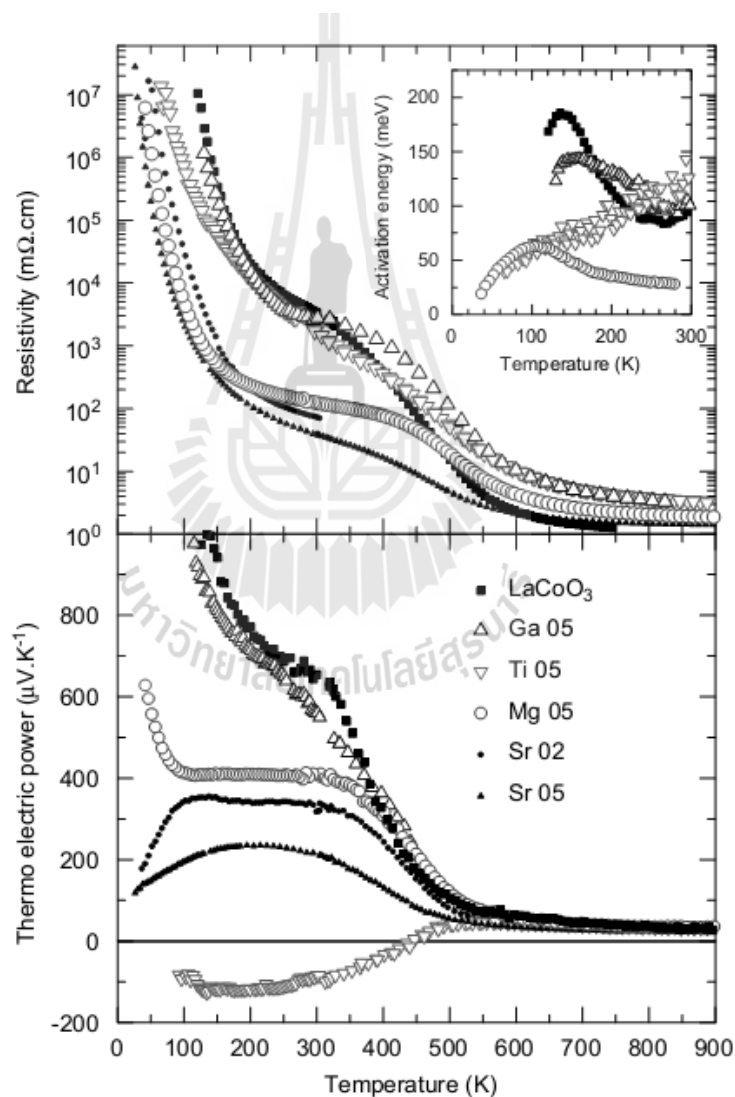**Figure 2.12** The electrical resistivity and the thermopower for $LaCo_{1-x}M_xO_3$ (x = 0.02, 0.05) when M is Ga, Ti, Mg, and Sr compared to $LaCoO_3$. Inset shows activation energy in the low-temperature region (Hejtmánek *et al.*, 2008).

Regarding this equation, the substitution which enhances the charge carrier concentration will simultaneously increase electronic thermal conductivity (κ_E). Therefore, the alternative way is to reduce the lattice part of the thermal conductivity (κ_L). When all the phonons have a mean free path intrinsically equal to the interatomic spacing of the constituent atoms, scattering phonons is attempted by creating rattling structures, alloying, grain-boundary scattering (due to the size of the grains) or point defects such as interstitials and vacancies (Snyder and Toberer, 2008; Tritt and Subramanian, 2006).

There have been several investigations into the enhancement of short wave phonon scattering by point defects; for example, Sr-(Zhou *et al.*, 2006), Pb-, and Na-substitution (He *et al.*, 2006) lower thermal conductivity of $LaCoO_3$. Iwasaki *et al.* (2008), however, discovered that the thermal conductivity reduction of Sr-doping is limited with the doping concentration range of 0-0.04; when Sr content is increased (0.05-0.4), the values increase with amount of carriers (Figure 2.13). Likewise, Ni doping up to 0.2 showed increasing thermal conductivity (Li and Li, 2011).

Apart from conventional ceramic method, Iwasaki *et al.* (2008) prepared $La_{1-x}Sr_xCoO_3$ with a polymerized complex method and found that thermal conductivity was improved depending on Sr concentration in the range of 0-0.2 (Zhou *et al.*, 2008b). These results show that the thermal conductivity mainly comes from its morphology structure. This implies that it is possible to increase the figure of merit ZT by optimizing compositions and microstructure in order to enhance phonon scattering, hence reduce thermal conductivity (Zhou *et al.*, 2008b). Other solution methods and sol-gel method were carried out to investigate the changes of thermal conductivity comparing to solid state reaction. Although the samples prepared by sol-gel processes

have better homogeneity and smaller average particle size, they have higher thermal conductivity than that of a solid state reaction because of their higher density. However, large ZT value of 0.046 is obtained in sol-gel sample of $La_{0.9}Sr_{0.1}CoO_3$ at room temperature (Zhou *et al*., 2008a).
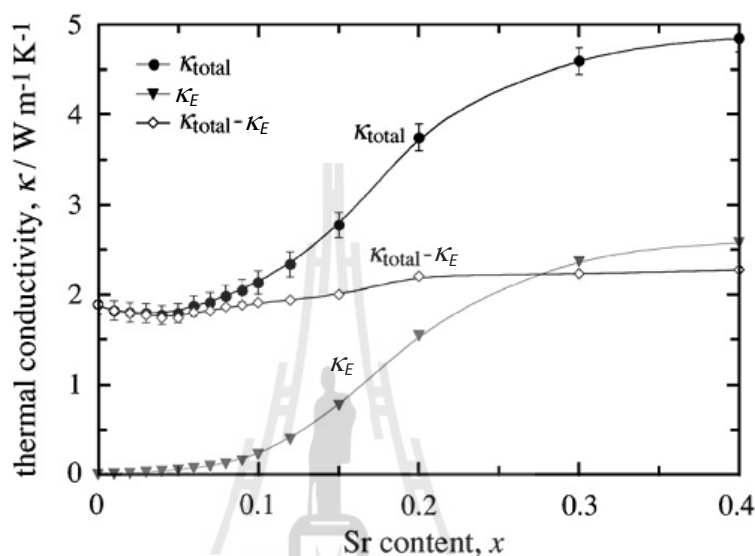
Figure 2.13 Thermal conductivity of $La_{1-x}Sr_xCoO_3$ dependence of Sr content at 300 K (Iwasaki *et al.*, 2008)
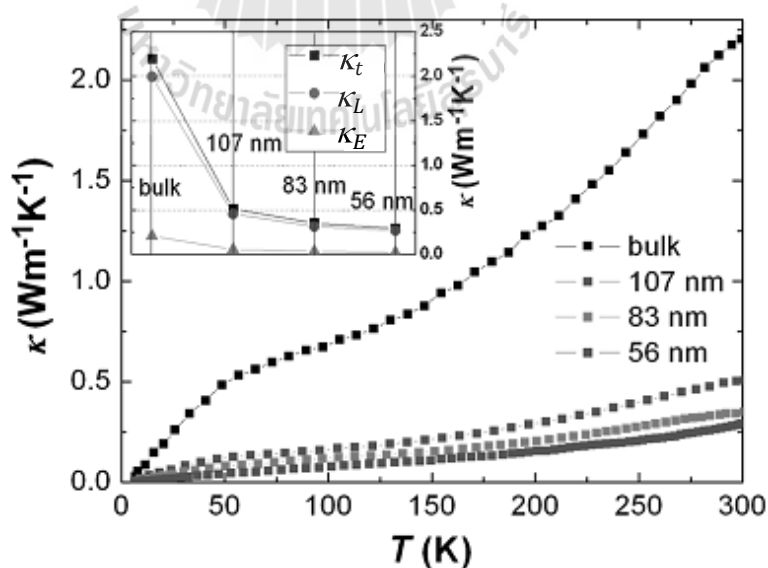
Figure 2.14 Temperature dependence of the thermal conductivity, κ, of the bulk and nanowires $La_{0.9}Sr_{0.1}CoO_3$. The inset presents the room-temperature κ_t, κ_L, and κ_E (Wang and Fan, 2010).

In addition, a hydrothermal method was used to prepare thermoelectric samples by Wang and Fan (2010). The nanowire samples exhibit strong suppression of thermal conductivity (Figure 2.14) and the samples with optimal size have a ZT value which is nearly two time higher than that of the bulk (Figure 2.15) (Wang and Fan, 2010).
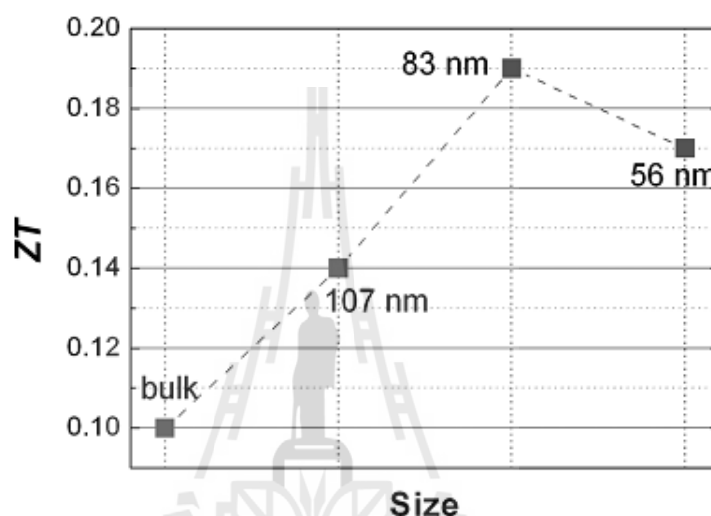
Figure 2.15 Plot of the ZT value versus the size of $La_{0.9}Sr_{0.1}CoO_3$ (Wang and Fan, 2010).

2.2.2.4 ZT improvement strategy

Since $LaCoO_3$-based oxides have been studied extensively for decades, the state-of-the-art researches are to maximize the dimensionless figure of merit ZT by substitutions. However, most works have mainly focused on single substitution for the La or Co site which leads to improvement of only one or two parameters against the other(s). As each substitution has different effects, the new idea of the double substitutions was introduced in an attempt to maximize the positive effects on as many parameters as possible.

In initial attempts, Sr substitution for La site and Mn substitution for Co site, $La_{0.80}Sr_{0.20}Co_{1-y}Mn_yO_3$ (y = 0.01-0.10) were conducted. Sr plays an important

role in enhancing electrical conductivity while Mn can both increase Seebeck coefficient and reduce thermal conductivity. As a result, a large ZT was obtained at room temperature (Suzuki *et al*., 2003). After that, $La_{0.95}Sr_{0.05}Co_{1-x}Rh_xO_3$ (x = 0.1-0.3) was also prepared. In spite of a slight increase in resistivity, Rh together with Sr can maintain Seebeck coefficient and remarkably reduce thermal conductivity providing a new route to achieve a higher ZT at higher temperatures (300-800 K) (Kwong *et al.*, 2010). Lately, double substitution in the same site, $LaCo_{0.8}(Ni_{0.1}Fe_{0.1})O_3$, showed improved transport properties and exhibits the great thermoelectric efficiency with ZT of 0.16 at room temperature (Vulchev *et al.*, 2012).

These findings provide new insights into an improvement of the thermoelectric perovskite oxides. The concept of the double substitution as well as sample preparation method will be very useful in achieving high thermoelectric efficiency of $LaCoO_3$-based oxides.

2.3 References

Androulakis, J., Migiakis, P., and Giapintzakis, J. (2004). $La_{0.95}Sr_{0.05}CoO_3$: An efficient room-temperature thermoelectric oxide. **Appl. Phys. Lett.** 84: 1099-1101.

Berggold, K., Kriener, M., Zobel, C., Reichl, A., Reuther, M., Müller, R., Freimuth, A., and Lorenz, T. (2005). Thermal conductivity, thermopower, and figure of merit of $La_{1-x}Sr_xCoO_3$. **Phys. Rev. B.** 72: 155116.

Chaikin, P. M. and Beni. G. (1976). Thermopower in the correlated hopping regime. **Phys. Rev. B.** 13: 647-651.

Goldschmidt, V. M. (1926). The laws of crystal chemistry. **Naturwissenschaften.** 14:

477-485.

Goodenough J. B. and Longo J. M. (1970). Magnetic properties of perovskite and perovskite related compounds. Springer: New York, USA.

He, T., Chen, J., Calvarese, T. G., and Subramanian, M. A. (2006). Thermoelectric properties of $La_{1-x}A_xCoO_3$ (A = Pb, Na). **Solid State Sci.** 8: 467-469.

He, J., Liu. Y., and Funahashi, R. (2011). Oxide thermoelectrics: the challenges, progress, and outlook. **J. Mater. Res.** 26: 1762-1772.

Hejtmánek, J., Jirák, Z., Knižek, K., Maryško, K., Veverka, M., and Fujishiro, H. (2004). Magnetism, structure and transport of $Y_{1-x}Ca_xCoO_3$ and $La_{1-x}Ba_xCoO_3$. **J. Magn. Magn. Mater.** 272–276: e283-e284.

Hejtmánek, J., Jirák, Z., Knížek, K., Maryško, M., Veverka, M., and Autret, C. (2008). Valence and spin states in perovskites $LaCo_{0.95}M_{0.05}O_3$ (M = Mg, Ga,Ti). **J. Magn. Magn. Mater.** 320: e92-e95.

Hébert, S., Flahaut, D., Martin, C., Lemonnier, S., Noudem, J., Goupil, C., Maignan, A., and Hejtmanek, J. (2007). Thermoelectric properties of perovskites: sign change of the Seebeck coefficient and high temperature properties. **Prog. Solid State Ch.** 35: 457-467.

Iwasaki, K., Ito, T., Nagasaki, T., Arita, Y., Yoshino, M., and Matsui, T. (2008). Thermoelectric properties of polycrystalline $La_{1-x}Sr_xCoO_3$. **J. Solid State Chem.** 181: 3145-3150.

Johnsson, M. and Lemmens, P. (2007). Crystallography and chemistry of perovskites. Handbook of magnetism and advanced magnetic materials. Edited by Helmut Kronmüller and Stuart Parkin. Volume 4: **Novel Materials.**

Koshibae, W., Tsutsui, K., and Maekawa, S. (2000) Thermopower in cobalt oxides.

Phys. Rev. B. 62: 6869-6872.

Kozuka, H., Ohbayashi, K., and Koumoto, K. (2012). $LaCo_{1-x}Ni_xO_3$ with improved electrical conductivity. **Inorg. Chem.** 51: 9259-9264.

Kwong, K.-S., Smith, A. E., and Subramanian, M. A. (2010). The effect of Rh and Sr substitution on the thermoelectric performance of $LaCoO_3$. **Mater. Res. Soc. Symp. Proc.** 1267: 1267-DD11-02.

Li, J., Smith, A. E., Kwong, K.-S., Powell, C., Sleight, A. W., and Subramanian, M. A. (2010). Lattice crossover and mixed valency in the $LaCo_{1-x}Rh_xO_3$ solid solution. **J. Solid State Chem.** 183: 1388-1393.

Li, F. and Li, J.-F. (2011). Effect of Ni substitution on electrical and thermoelectric properties of $LaCoO_3$ ceramics. **Ceram. Int.** 37: 105-110.

Maignan, A., Caignaert, V., Raveau, B., Khomskii, D., and Sawatzky, G. (2004). Thermoelectric power of $HoBaCo_2O_{5.5}$: possible evidence of the spin blockade in cobaltites. **Phys. Rev. Lett.** 93: 026401-1-4.

Mandal, P., Choudhury, P., Biswas, S. K., and Ghosh, B. (2004). Transport and magnetic properties of $La_{1-x}Ba_xCoO_3$. **Phys. Rev. B.** 70: 104407-1-104407-8.

Mandal, P., Choudhury, P., and Ghosh, B. (2005). Transport studies of metallic $La_{1-x}A_xCoO_3$ (A = Sr, Ba) ferromagnet. **Physica B.** 359-361: 1363-1365.

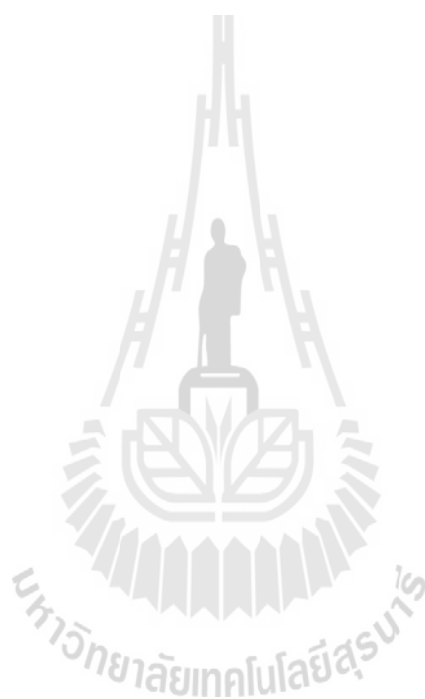Mitchell, R. H. (2002). Perovskites-modern and ancient, Alamaz Press Inc.: Ontario, Canada.

Mineshige, A., Kobune, M., Fujii, S., Ogumi, Z., Inaba, M., Yao, T., and Kikuchi, K. (1999). Metal-insulator transition and crystal structure of $La_{1-x}Sr_xCoO_3$ as functions of Sr-content, temperature, and oxygen partial pressure. **J. Solid State Chem.** 142: 374-381.

Ohtaki, M. (2011). Recent aspects of oxide thermoelectric materials for power generation from mid-to-high temperature heat source. **J. Ceram. Soc. Jpn.** 119: 770-775.

Peltier, J. C. (1834). Novelles experiences sur la caloriecete des courans electriques. **Anm. Chem.** 371-387.

Ramadass, N., Gopalakrishnan, J., and Sastri, M.V.C. (1979). Studies on magnesium- and titanium-substituted $LaCoO_3$. **J. Less-Common. Met.** 65: 129-138.

Robert, R., Bocher, L., Trottmann, M., and Weidenkaff, A. (2006). Synthesis and high-temperature thermoelectric properties of Ni and Ti substituted $LaCoO_3$. **J. Solid State Chem.** 179: 3893-3899.

Robert, R., Bocher, L., Sipos, B., Döbeli, M., and Weidenkaff, A. (2007). Ni-doped cobaltates as potential materials for high temperature solar thermoelectric converters. **Prog. Solid State Ch.** 35: 447-455.

Robert, R., Aguirre, M. H., Bocher, L., Trottmann, M., Heiroth, S., Lippert, T., Döbeli, M., and Weidenkaff., A. (2008). Thermoelectric properties of $LaCo_{1-x}Ni_xO_3$ polycrystalline samples and epitaxial thin films. **Solid State Sci.** 10: 502-507.

Robert, R., Logvinovich, D., Aguirre, M. H., Ebbinghaus, S. G., Bocher, L., Tomeš, P., and Weidenkaff, A. (2010). Crystal structure, morphology and physical properties of $LaCo_{1-x}Ti_xO_{3\pm\delta}$ perovskites prepared by a citric acid assisted soft chemistry synthesis. **Acta. Mater.** 58: 680-691.

Seebeck, T. J. (1823). Magnetische polarisation der metalle und erze durck temperatur-differenz. **Abh. K. Akad. Wiss.** 265-373.

Señarís-Rodríguez, M. A. and Goodenough, J. B. (1995). $LaCoO_3$ revisited. **J. Solid State Chem.** 116: 224-231.

Snyder G. J. and Toberer E. S. (2008). Complex thermoelectric materials. **Nat. Mater.** 7: 105-114.

Suzuki, K., Fujishiro, H., Kashiwada, Y., Fujine, Y., and Ikebe, M. (2003). Magnetic, electrical and thermal properties of $La_{0.80}Sr_{0.20}(Mn_yCo_{1-y})O_3$. **Physica B.** 329-333: 922-923.

Tejuca., L. G. and Fierro., J. L. G. (1989). Structure and reactivity of perovskite-type oxides. **Adv. Catal.** 36: 237-328.

Tritt, T. M. and Subramanian, M. A. (2006). Thermoelectric materials, phenomena, and applications: a bird's eye view. **Mater. Res. Bull.** 31: 188-198.

Vulchev, V., Vassilev, L., Harizanova, S., Khristov, M., Zhecheva, E., and Stoyanova, R. (2012). Improving of the thermoelectric efficiency of $LaCoO_3$ by double substitution with nickel and iron. **J. Phys. Chem. C.** 116: 13507-13515.

Wang Y. and Fan. H. J. (2010). Improved thermoelectric properties of $La_{1-x}Sr_xCoO_3$ nanowires. **J. Phys. Chem. C.** 114: 13947-13953.

Weidenkaff, A., Robert, R., Aguirre, M., Bocher, L., Lippert, T., and Canulescu, S. (2008). Development of thermoelectric oxides for renewable energy conversion technologies. **Renew. Energ.** 33: 342-347.

Zhou, A. J., Zhu, T. J., and Zhao, X. B. (2006). Thermoelectric properties of perovskite-type oxide $La_{1-x}Sr_xCoO_3$ (x = 0, 0.1) prepared by solid state reactions. **Mater. Sci. Eng**. **B.** 128: 174-178.

Zhou, A. J., Zhu, T. J., Zhao, X. B., Chen, H. Y., and Müller, E. (2008a). Fabrication and thermoelectric properties of perovskite-type oxide $La_{1-x}Sr_xCoO_3$ (x = 0, 0.1). **J. Alloy. Compd.** 449: 105-108.

Zhou, A. J., Zhu, T. J., and Zhao, X. B. (2008b). Thermoelectric properties of

perovskite oxides $La_{1-x}Sr_xCoO_3$ prepared by polymerlized complex method. **J. Mater. Sci.** 43: 1520-1524.

CHAPTER III

EXPERIMENTAL

3.1 Chemicals

- Citric acid monohydrate ($C_6H_8O_7 \cdot H_2O$), 99.5-105.5%, Carlo Erba

- Cobalt(II) nitrate hexahydrate ($Co(NO_3)_2 \cdot 6H_2O$), 99+%, Acros Organic

- Lanthanum(III) nitrate hexahydrate ($La(NO_3)_3 \cdot 6H_2O$), 99.999%, Acros Organic

- Magnesium(II) nitrate ($Mg(NO_3)_3 \cdot 4H_2O$), 99.5%, Qrëc

- Strontium(II) nitrate ($Sr(NO_3)_2$), 99+%, Acros Organic

3.2 Instruments

- Simultaneous thermal analyzer (STA), Model STA449 F3, NETZSCH

- Fourier transform infrared spectrometer (FT-IR), Model Spectrum GX, Perkin-Elmer

- Powder X-ray diffractometer (XRD), Model D2 Phaser, Bruker

- Field emission scanning electron microscope (FESEM), Model JSM-7800F, JEOL/Energy dispersive X-ray spectroscopy (EDS), Model X-Max 50 mm, Oxford instruments

- Physical properties measurement system (PPMS), Quantum Design

3.3 Sample preparation

3.3.1 Sol-gel method

Sol-gel method is a good method to improve homogeneity of a sample as the reagents are well-mixed on an atomic scale. The precursors of metal salts are dissolved giving a colloidal solution named 'sol'. The gel can be formed by a dehydration process of the sol. After drying and calcination, a final product is obtained. Another good point of this preparation technique is that heating temperature is usually decreased (Segal, 1997).

In this work, polycrystalline samples of $La_{1-x}Sr_xCoO_3$, $LaCo_{1-x}Mg_xO_3$ (x = 0, 0.02, 0.05, 0.1, 0.2), and $La_{1-x}Sr_xCo_{1-x}Mg_xO_3$ (x = 0, 0.025, 0.05, 0.1) were prepared by the citrate sol-gel method. High purity starting materials of $La(NO_3)_3 \cdot 6H_2O$, $Co(NO_3)_2 \cdot 6H_2O$, $Sr(NO_3)_2$, and $Mg(NO_3)_2 \cdot 6H_2O$ were weighed in a stoichiometric ratio and dissolved in a citric acid solution with 1:4 molar ratio (cations:citric acid). The aqueous solution was heated with constant stirring at 353 K for 2 hours resulting in a red transparent solution. Then the solution was dried at 393 K in air in an oven overnight to transform into a dried gel. The obtained dried gel was ground and calcined at 1023-1073 K for 8-12 hours at a heating rate of 5 K/min to give a black powder. The calcined powder was ground, pressed into a pellet, and then sintered at 1273 K for 24 hours in air. A bar-shaped sintered-pellet with general dimensions of about 10 mm x 3 mm x 2 mm was prepared for the thermoelectric properties measurement

3.4 Characterizations

3.4.1 Structure identifications

3.4.1.1 Thermogravimetry/Differential thermal analysis (TG/DTA)

Thermogravimetric technique monitors the change in weight of a sample as a function of temperature or time in a controlled atmosphere. Each change in weight refers to the decomposition of the components of a compound at each temperature. When the compounds have no change, weight of a sample remains constant with increasing temperature. In this study, thermogravimatry analysis (TGA) was used to investigate the decomposition of substances and to find the temperature required to decompose all organic species in the samples prepared by the sol-gel method in order to determine the calcining temperature.

Differential thermal analysis technique measures the difference in temperature, ΔT, between a sample and an inert reference material as a function of temperature; therefore, detects changes in heat content, that is, enthalpy. Changes in samples relative to the reference are either endothermic or exothermic. Thus, a DTA curve provides data on the heat changes that an involved chemical reaction have. The DTA curve was utilized for this purpose in this study.

Thermal decomposition of the dried gels was investigated by TG/DTA using a NETZSCH STA449 F3 Simultaneous Thermal Analyzer instrument (STA). The dried gel was put in an Al_2O_3 crucible and heated from 303 K to 1273 K with a heating rate of 10 K/min under the atmosphere of 80% nitrogen and 20% oxygen.

3.4.1.2 Fourier transform infrared spectrometer (FT-IR)

This spectroscopic technique is related with the infrared radiation; some of infrared radiation is absorbed by the sample and some of it is transmitted. The absorption of infrared at specific frequencies is characteristic to vibrations between bonds of the atoms. An infrared spectrum represents a fingerprint of a sample and can be shown in either the absorption or transmission mode.

In this study, FT-IR was used to probe the structural information of the samples. The presence of specific peaks in the infrared spectra was used to confirm the functional groups of the obtained products.

In the experiment, FT-IR spectra were obtained by a model spectrum GX Perkin-Elmer IR spectrometer. The sample was mixed with dry KBr and pressed to form a pellet for the measurement. Spectra were collected in the range 4000-400 cm^{-1} using 32 scans with a resolution of 4 cm^{-1}.

3.4.1.3 X-ray diffraction (XRD)

X-ray diffraction is a principal technique of solid state chemistry, which is widely used for crystal structure determination and phase identification. In principle, a monochromatic beam of X-rays, which strikes the powder of a solid, interacts with electrons in matter in which it is scattered in various directions by the electron cloud of the atoms. Referring Bragg's equation ($n\lambda = 2d\sin\theta$), the constructive interferences occurred with scattered X-rays which are in phase and contribute to X-ray powder diffraction patterns. Each solid material has its own characteristic X-ray powder diffraction pattern.

In this study, the X-ray powder diffraction patterns were used as a fingerprint of samples for phase identification and phase purity confirmation. When a

pure phase of a compound is obtained, the investigation of a crystal structure is necessary. Crystallographic information such as cell parameters can be calculated from positions or *d*-spacings of the set of peaks.

In this work, XRD patterns of all samples were collected at room temperature on a model D2 Phaser of Bruker X-ray diffractometer. To check a phase purity, the operation uses Cu Kα radiation (λ=0.15406 Å) with 30 mV and 10 mA scanning in diffraction angle (2θ) range of 20-80˚ at the rate of 0.5˚/s and the increment of 0.02˚. The phase identification and the crystal structure were determined using PDF-2 (2004) database and EVA software. To analyze unit cell parameters of the samples, the Le Bail structure refinement method was performed with TOPAS software using the high quality XRD patterns collected with the diffraction angle (2θ) from 20˚ to 120˚ using the increment of 0.01 at the scan speed of 1˚/s.

3.4.1.4 Field Emission Scanning Electron Microscope (FESEM)/

Energy Dispersive X-ray Spectroscopy (EDS)

This electron microscopy provides the microstructural information on the surface of a sample. In FESEM, the gun typed field emission (FE) is applied which gives an electron beam with high-brightness and better focus. With the same principle as other SEM, a sample is bombarded with high-energy electrons from a source called electron gun. A secondary electron is generated to construct the image of a sample's morphology. By the electron bombardment, X-ray energy is also produced by the replacement of an outer-shell electron for a hole when an absorbed electron is rejected out of an atom. This characteristic X-ray emission relates to the type of an atom and is detected in EDS technique. Thus, a quantitative analysis of an element can be investigated (Smart and Moore, 2005; West, 2014).

The purpose of this study was to determine the amount of each element in the sample. The sintered bars of all samples were coated with a layer of gold to make them electrically conduct. All FESEM images were taken with a magnification of 5,000 to 30,000 using the accelerating voltage of 15 kV. A working distance of 10 mm was used with a resolution of 1 nm. By using EDS, the point and ID analysis was performed to capture the interested area of the image to study an elemental composition.

3.4.2 Thermoelectric properties characterizations

Thermoelectric measurements, including electrical resistivity (ρ), Seebeck coefficient (S), and thermal conductivity (κ), were performed on sintered pellets in a Quantum Design Physical Properties Measurement System (PPMS) coupled with the thermal transport option (TTO). The measurements were done at room temperature. The dimensionless thermoelectric figure of merit, ZT, was determined based on the algebraic combination, $ZT = (S^2/\rho\kappa)T$.

3.4.2.1 Physical properties measurement system (PPMS)

Electrical resistivity is one of the important transport properties of a material which is used to determine how well the material can electrically conduct. Moreover, the range of electrical resistivity indicates the type of materials as insulator, semiconductor, or metal (Elsheikh *et al*., 2014). With the TTO system, a digital signal processor (DSP) current is used as a source and phase sensitive voltage is used as a detection system. The standard four-probe method is employed for the measurement with AC transport mode. The advantage of the four-probe method is that it can prevent the problem from a contact resistance occurred in a two-probe configuration (Quantum Design, 2002).

Seebeck coefficient provides the information about the thermal diffusion of free charge carriers, which can be an electron or a hole. According to the Seebeck effect, charge carrier diffusion generates an electric field inside a material which creates a voltage gradient when a temperature gradient is applied. The TTO system measures Seebeck coefficient by originating a particularized temperature difference (ΔT) and monitoring an electrical voltage difference (ΔV) (Quantum Design, 2002). The ratio of these two measured parameters ($\Delta V/\Delta T$) is equal to S (Tritt and Subramanian, 2006).

The measurement of thermal conductivity evaluates the ability of a material to conduct heat. In the TTO system, the heater source applies heat to a sample and the amount of heat passes through the sample is collected from the observed temperature drop. Thus, thermal conductivity can be calculated directly from three parameters: an applied heater power, a resulting ΔT, and a sample dimension (Quantum Design, 2002).
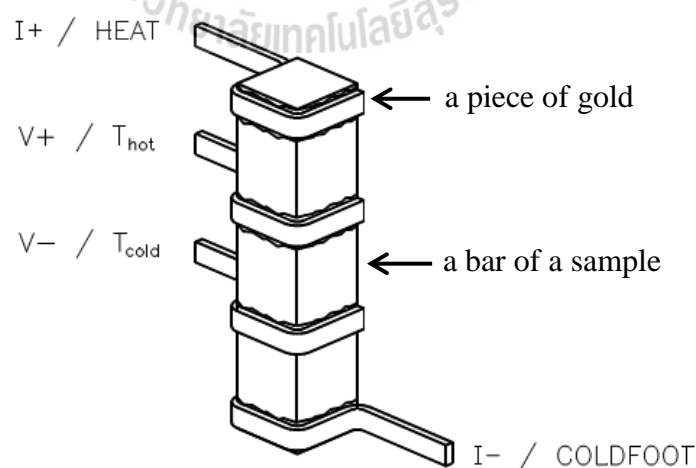

Figure 3.1 The sample preparation for the four-probe measurement (Quantum Design, 2002).

The samples were prepared for a four-probe measurement. The bars of all samples were mounted with four rectangular pieces of gold using an electrically conducting silver-filled epoxy (Figure 3.1). Then, they were undergone baking at about 423 K for around 5 minutes to allow all pieces of gold to attach properly to the surface of samples. To set up a sample for the measurement, firstly, the prepared bar
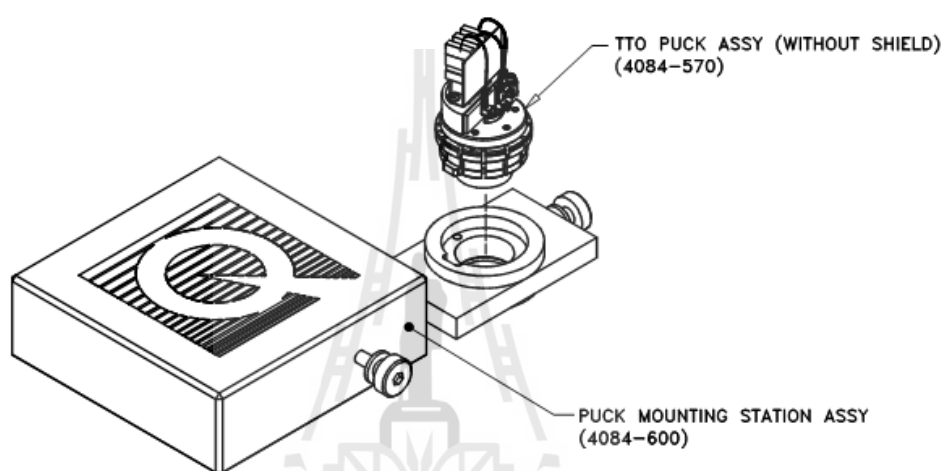

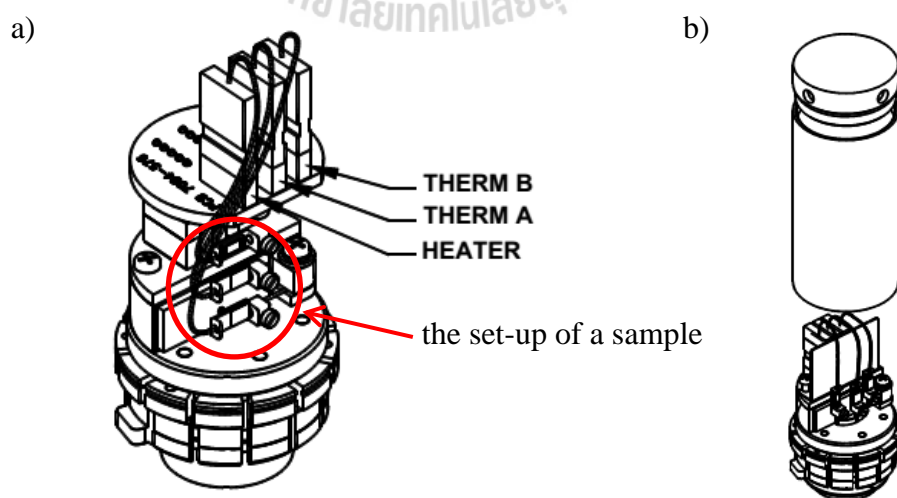**Figure 3.2** The puck-mouting station for a sample preparation (Quantum Design, 2002)

Figure 3.3 The thermal transport sample puck (TTO puck) demonstrating (a) the set up of a sample, (b) TTO puck with a radiation shield (Quantum Design, 2002).

of samples was set into the thermal transport sample puck (TTO puck) (Figure 3.3a) using the puck-mounting station (Figure 3.2). Then, the TTO puck was plugged into the puck-wiring test station in order to check an electrical contact by checking contact at V+/V- and I+/I- with an ohmmeter. After that, the TTO puck was covered with a radiation shield (Figure 3.3b) and then was plugged into the 12-pin socket which is located at the bottom of the PPMS sample chamber (Quantum Design, 2002).

The measurement was done under hi-vacuum system and controlled by the TTO software. Electrical resistivity (ρ), Seebeck coefficient (S), and thermal conductivity (κ), were measured simultaneously and the figure of merit ZT was calculated. By using the TTO software, the units of all parameters were recorded as Ω-m, μVK^{-1}, and $Wm^{-1}K^{-1}$ for ρ, S, and κ, respectively. So, ZT is reported as dimensionless (Quantum Design, 2002).

3.5 References

Elsheikha, M. H., Shnawah, D. A., Sabri, M. F. M., Said, S. B. M., Hassan, M. H., Bashir, M. B. A., and Mohamad, M. (2014). A review on thermoelectric renewable energy: principle parameters that affect their performance. **Renew. Sust. Energ. Rev.** 30: 337-355.

Quantum Design. (2002). Physical properties measurement system: thermal transport option user's manual.

Segal, D. (1997). Chemical Synthesis of Ceramic Materials. **J. Mater. Chem.** 7(8): 1297-1305.

Smart, L. E. and Moore, E. A. (2005). **Solid state chemistry: An introduction** (3rd ed.). Boca Raton: Taylor & Francis group.

Tritt, T. M. and Subramanian, M. A. (2006). Thermoelectric materials, phenomena, and applications: a bird's eye view. **Mater. Res. Bull.** 31: 188-198.

West, A. R. (2014). **Solid state chemistry and its applications** (2nd ed.). West Sussex: John Wiley & Sons Inc.
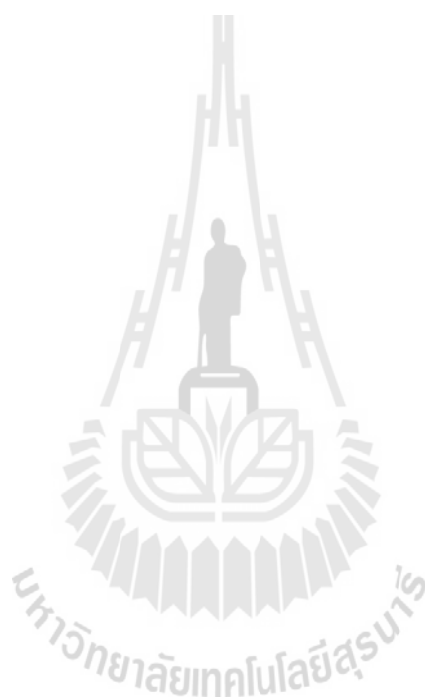
CHAPTER IV

RESULTS AND DISCUSSION

4.1 Sample preparation

In this work, all samples of $LaCoO_3$-based oxides, which are $La_{1-x}Sr_xCoO_3$, $LaCo_{1-x}Mg_xO_3$ (x = 0, 0.02, 0.05, 0.1, 0.2), and $La_{1-x}Sr_xCo_{1-x}Mg_xO_3$ (x = 0, 0.025, 0.05, 0.1), were synthesized by the citrate sol-gel method. The sol-gel technique involves four main mechanisms: hydrolysis, polymerization, drying, and densification (Rao and Raveau, 1988). In case of metal oxides, a metal alkoxide is normally used as a precursor (Put, 1998). In this experiment, a citric acid was used as a chelating ligand to form the metal alkoxide (Predoana *et al*., 2009). The mechanism of $LaCoO_3$ was proposed by Predoana *et al*. (2009), that of Sr-doped and Mg-doped $LaCoO_3$ in this work can be proposed based on the same way as shown in following steps:

Firstly, the starting materials of metal nitrates were dissolved in water producing a small particle of metals suspended in an aqueous solution, a system called "sol" (Rao and Raveau, 1988). A metal is solvated by six molecules of water resulting in the hydrate form. This process is called "hydrolysis".

Secondly, with the presence of citric acids, the water condensation of the metal hydrate is occurred. Citric acids begin to chelate with metal ions forming the coordination compound. This corresponds to "gel" formation because of the aggregation of those particles in the sol (Rao and Raveau, 1988).

Then, the condensation proceeds continuously as citric acids chelate all metals

forming the complex. The metal network is growing during this process and this step is, therefore, called "polymerization".

After that, the metals-citric acid chelate dries resulting in a dried gel, xerogel or aerogel, depending on the purpose of applications (Rao and Raveau, 1988). Finally, the densification procedure, such as pelletizing and sintering, is applied for specific uses. (Livage et al., 1988)

4.2 Sample characterization

4.2.1 Thermogravimatry/Differential thermal analysis (TG/DTA)

Thermal behavior of the $La_{0.975}Sr_{0.025}Co_{0.975}Mg_{0.025}O_3$ dried gel was investigated by TG/DTA (Figure 4.1). As all the samples are $LaCoO_3$-based oxides, $La_{0.975}Sr_{0.025}Co_{0.975}Mg_{0.025}O_3$ was used as a representative. The mechanism of phase changes of dried gel precursor was investigated by weight loss (%) as a function of temperature from 303 K to 1273 K. The weight changes are observed at temperature lower than 873 K which are related to the thermal decompositions of water, citrate precursors, carbon monoxide, and carbon dioxide (Robert *et al*., 2007). There was no weight loss observed at higher temperature. There are approximately three stages of weight loss. The first endothermic loss of weight occurred at 303-453 K is related to the evaporation of crystalline water. The major weight loss was observed between 453 K and 643 K, which corresponds to the decomposition of citrate precursors (Robert *et al*., 2007). Changes in DTA at these temperatures are small which suggests that these reactions involved much smaller energy changes compared with those at the last stage. The last stage of weight loss of 27.25% at 723 K accompanied by a strong exothermic DTA peak is ascribed to the loss of remaining organic components, where carbon

monoxide and carbon dioxide was released. As the measurement was performed under $80\%N_2/20\%O_2$ atmosphere, decomposed organic species combusted in the presence of oxygen giving the large exothermic DTA peak (Wu *et al*., 2011). The weight loss steps from TGA along with the DTA peaks show that the stepwise thermal decomposition of the precursors completes at 873 K. The total weight loss was 78.02%.
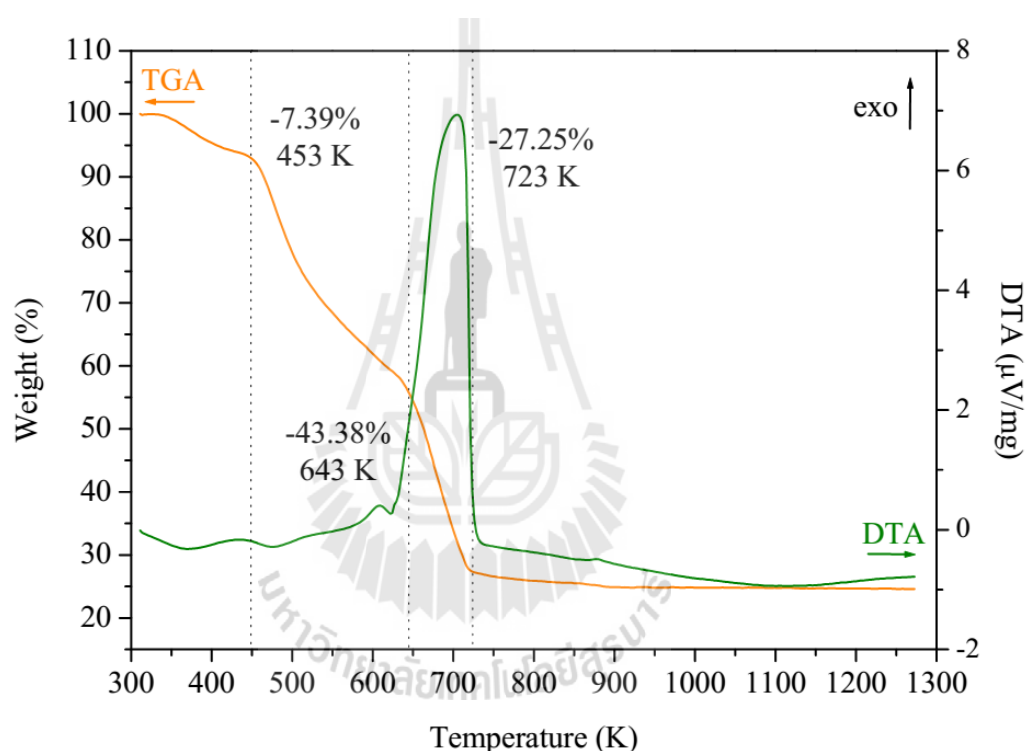

Figure 4.1 TG/DTA curves of the dried gel $La_{0.975}Sr_{0.025}Co_{0.975}Mg_{0.025}O_3$.

4.2.2 Fourier transform infrared spectrometer (FT-IR)

Figure 4.2 shows the FT-IR spectra of the $La_{0.975}Sr_{0.025}Co_{0.975}Mg_{0.025}O_3$ samples. The observed peaks are assigned to vibrations of molecular bonds and indexed as shown in the figure. The FT-IR spectrum of citric acid shows functional groups characteristics of carboxylic group. The broad band around 3433 cm^{-1} is assigned to O-H stretching (Pavia *et al*., 2009), while the doublets at 1767 cm^{-1} and 1713 cm^{-1} are

attributed to stretching vibrations of free carboxylic groups and carboxylic groups forming intramolecular hydrogen bond, respectively (Cannas *et al*., 2006). Absorption bands at 1630 cm^{-1} and 1412 cm^{-1} are due to asymmetric and symmetric stretching of resonance $^{-}$O-C=O vibrations, respectively (Worayingyong *et al*., 2008). The FT-IR spectrum of the dried sample exhibits some similar absorption bands with lower intensities. The O-H stretching at 3433 cm^{-1} might belong to some free carboxylic group or moisture. The C=O and two $^{-}$O-C=O stretching vibrations shift to 1719 cm^{-1}, 1633 cm^{-1}, and 1407 cm^{-1}, respectively in the dried sample. These shifts indicate the coordination between metal ions and carboxylic group of citric acids (Predoana *et al*., 2009).
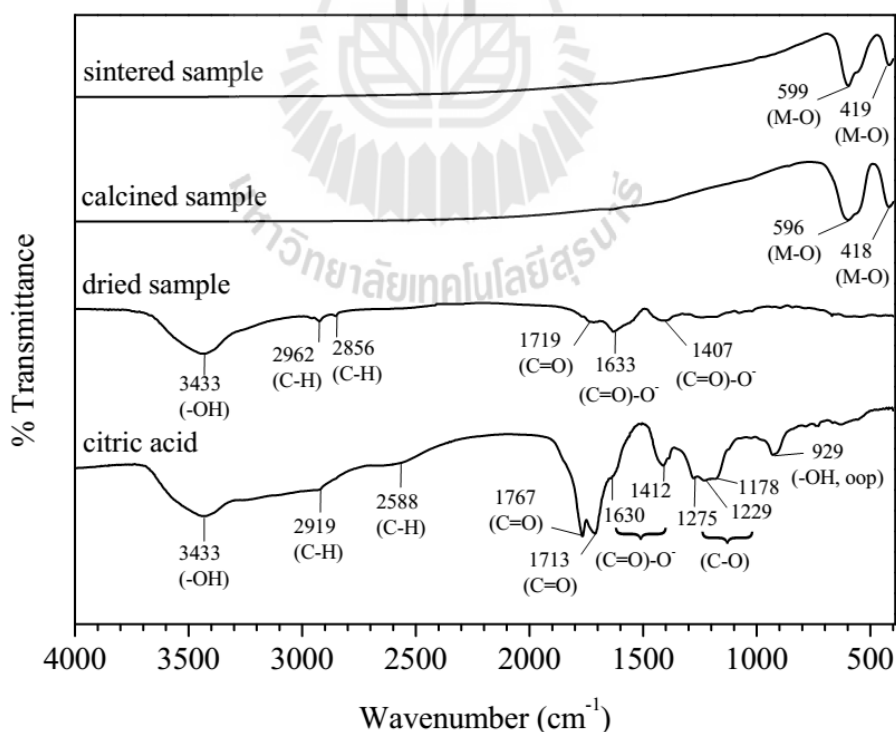

Figure 4.2 FT-IR spectrum of the dried gel, calcined, and sintered sample of La$_{0.975}$Sr$_{0.025}$Co$_{0.975}$Mg$_{0.025}$O$_3$, and citric acid.

The FT-IR spectrum of the calcined sample shows the evolution of the compound after a heat treatment at 1023 K. The spectrum presents the absence of the bands corresponding to the components of citrate precursors while metal-oxide bonds (M-O) vibrations around 400-600 cm^{-1} are observed which indicates the formation of oxides. The bands at 596 cm^{-1} (very strong) and 559 cm^{-1} (shoulder) are attributed to Co-O stretching while the band at 419 cm^{-1} (strong) corresponds to Co-O bending (Couzi and Huong, 1974; Merino *et al*., 2005). These bands are also detected at similar wavenumbers in the spectrum of the sintered sample. The fact that only bands for metal-oxide bonds are present in the calcined and sintered samples indicates that all organic species have completely decomposed.

4.2.3 X-ray diffraction (XRD)

The XRD patterns of sintered $La_{1-x}Sr_xCoO_3$ (x = 0.02, 0.05, 0.1, 0.2), $LaCo_{1-x}Mg_xO_3$ (x = 0.02, 0.05, 0.1, 0.2), and $La_{1-x}Sr_xCo_{1-x}Mg_xO_3$ (x = 0.025, 0.05, 0.1) samples are shown in Figures 4.3, 4.4, and 4.5, respectively. The diffraction peaks of all samples can be indexed as the $LaCoO_3$ phase which has a rhombohedral distorted-perovskite structure with the $R\bar{3}c$ space group (PDF 48-0123). The calculated cell parameters *a* and *c* are listed in Table 4.1. In general, the partial substitutions of Sr^{2+} for La^{3+} and Mg^{2+} for Co^{3+} cause increases in unit cell parameters because the ionic radii of Sr^{2+} (1.18 Å) and Mg^{2+} (0.72 Å) are greater than those of La^{3+} (1.032 Å) and Co^{3+} (0.545 Å for low-spin and 0.61 Å for high-spin configurations) (Shannon and Prewitt, 1969; Shannnon, 1976). The situation could be complicated, however, when the following two issues are taken into account. First, some Co^{3+} ions are oxidized to Co^{4+} ions with a smaller ionic radius (0.53 Å) to preserve the charge neutrality. Secondly, Co^{3+} in this system can be either in the high-,

intermediate-, or low-spin state or even in a mixture of them (Li *et al*., 2010; Kriener *et al*., 2004). As shown in Figure 4.6, the substitutions of both cations have more effects on cell parameter *c* than on cell parameter *a*, indicating that the unit cell elongates along the *c* axis with increasing cation substitution content. This tendency is similar to that observed in $La_{1-x}Sr_xCoO_3$ prepared by other works (Iwasaki *et al*., 2008; Mineshige *et al*., 1996). The plot of the *c*/*a* ratio is shown in Figure 4.6c to confirm that substitutions were successful (Zhou *et al*., 2008b).

Based on the ionic radius, Goldschmidt defined the tolerance factor (*t*), $t = (r_A+r_O)/\sqrt{2}(r_B+r_O)$, to determine the degree of a structural distortion of cubic perovskite (ABO$_3$). To illustrate the ideal perovskite structure, SrTiO$_3$ has *t* = 1; the calculation was done using $r_{A(Sr)}$ = 1.44 Å, $r_{B(Ti)}$ = 0.605 Å, and r_O = 1.40 Å (Wells, 2008; Müller, 1993). In case of LaCoO$_3$, B cation size is similar ($r_{B(Co)}$ = 0.545-0.61
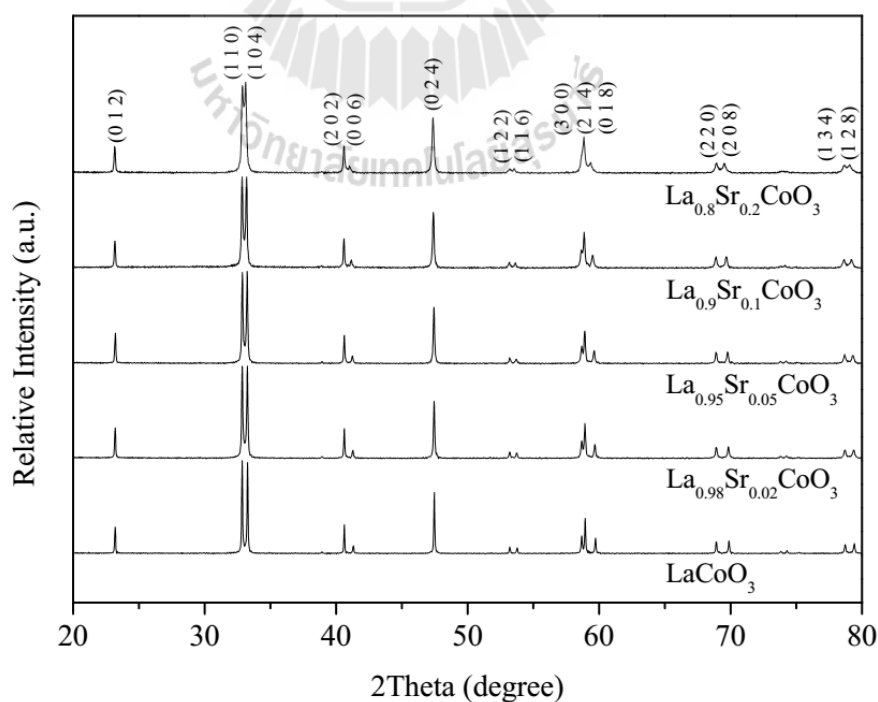
Figure 4.3 XRD patterns of $La_{1-x}Sr_xCoO_3$ (x = 0.02, 0.05, 0.1, 0.2).
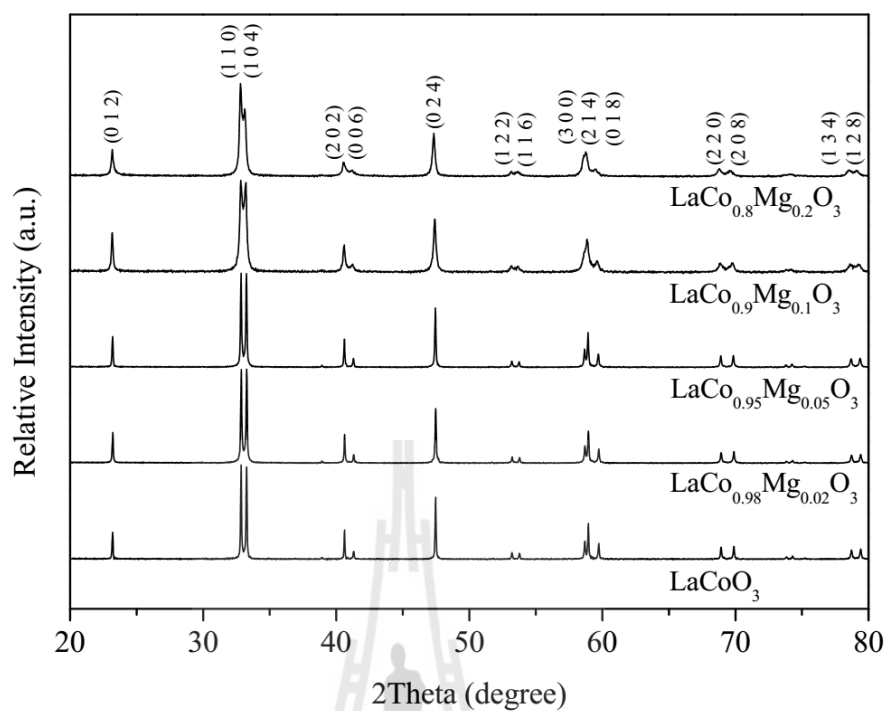
Figure 4.4 XRD patterns of $LaCo_{1-x}Mg_xO_3$ (x = 0.02, 0.05, 0.1, 0.2).

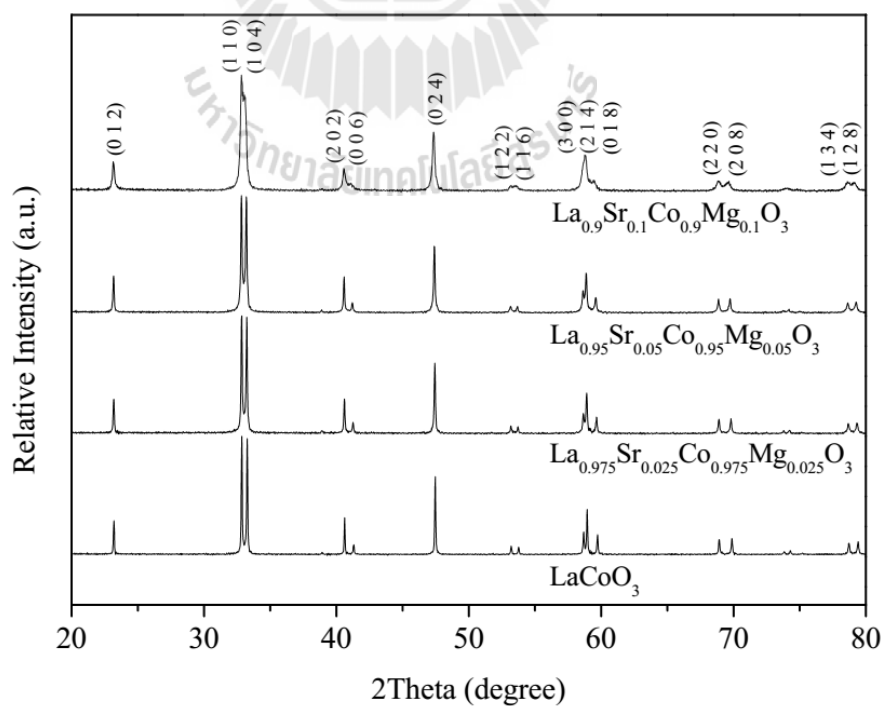**Figure 4.5** XRD patterns of $La_{1-x}Sr_xCo_{1-x}Mg_xO_3$ (x = 0.025, 0.05, 0.1).

Å) while A cation is smaller ($r_{A(La)}$ = 1.032 Å); therefore, *t* is less than 1. The smaller size of La causes CoO_6 octahedra to tilt, and thus the structure is distorted from a cubic to a rhombohedral distorted-perovskite structure. The double substitution of Sr and Mg, which have greater ionic radii, for La and Co should cause an increase in the *t* value which leads to a higher symmetry in the crystal structure (Johnsson and Lemmens, 2007). In fact, it has been reported that $La_{1-x}Sr_xCoO_3$ show a structure transformation from a rhombohedral (when x = 0-0.5) to a cubic structure (when 0.55 < x < 0.7) (Mineshige *et al.*, 1996). In our experiments, a change of symmetry with increasing x is also evident in the XRD patterns as two reflections near 33° are merging into one peak (Øygarden *et al.*, 2012).
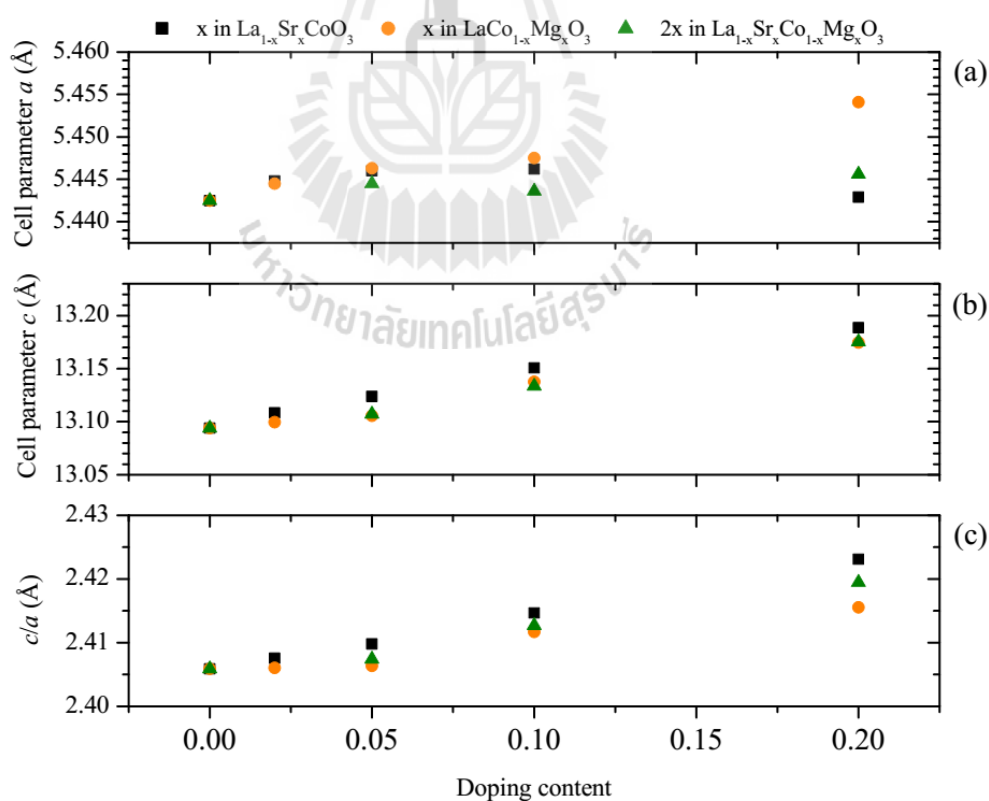

Figure 4.6 Cell parameters (a) *a* and (b) *c* and (c) the *c/a* ratio of $La_{1-x}Sr_xCoO_3$, $LaCo_{1-x}Mg_xO_3$, and $La_{1-x}Sr_xCo_{1-x}Mg_xO_3$.

Table 4.1 Cell parameters a and c of all samples calculated from TOPAS software.

Samples	a (Å)	c (Å)
$LaCoO_3$	5.4425	13.0940
$La_{0.98}Sr_{0.02}CoO_3$	5.4448	13.1085
$La_{0.95}Sr_{0.05}CoO_3$	5.4460	13.1238
$La_{0.9}Sr_{0.1}CoO_3$	5.4462	13.1508
$La_{0.8}Sr_{0.2}CoO_3$	5.4429	13.1887
$LaCo_{0.98}Mg_{0.02}O_3$	5.4445	13.0996
$LaCo_{0.95}Mg_{0.05}O_3$	5.4463	13.1057
$LaCo_{0.9}Mg_{0.1}O_3$	5.4475	13.1377
$LaCo_{0.8}Mg_{0.2}O_3$	5.4541	13.1746
$La_{0.975}Sr_{0.025}Co_{0.0975}Mg_{0.025}O_3$	5.4445	13.1072
$La_{0.95}Sr_{0.05}Co_{0.95}Mg_{0.05}O_3$	5.4436	13.1337
$La_{0.9}Sr_{0.1}Co_{0.9}Mg_{0.1}O_3$	5.4456	13.1754

4.2.4 Field Emission Scanning Electron Microscopy (FESEM)/Energy Dispersive X-ray Spectroscopy (EDS)

Morphology of the sintered samples was studied by FESEM technique. FESEM micrographs of all samples (Figure 4.7-4.18) show that particle sizes of the samples varying from 100 nm to 1 micron. The samples are homogeneous with a good particle distribution. The figures show spherical and/or random shape of particles which is resulted from the three dimensional structure of $LaCoO_3$-based compound. Compounds with layer structure often gives plate-like or sheet-like particle as the particles grow with certain plane preference. The images also indicate that the pellets have quite low density (about 80% of theoretical density).
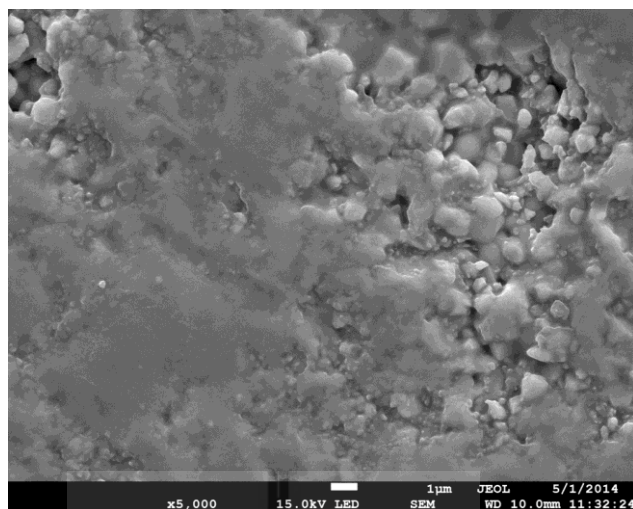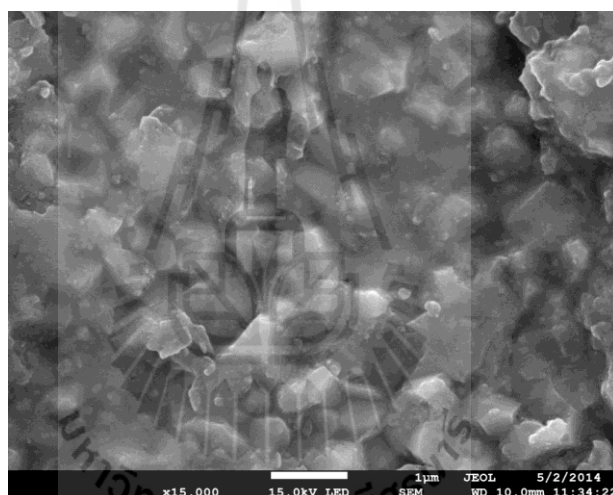
Figure 4.7 FESEM image of LaCoO$_3$.

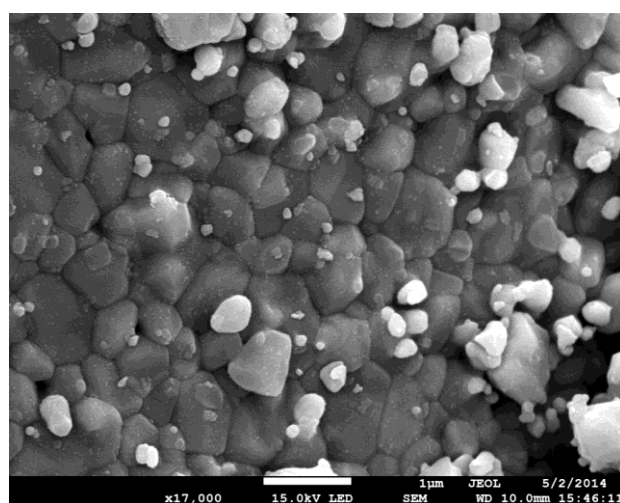**Figure 4.8** FESEM image of La$_{0.98}$Sr$_{0.02}$CoO$_3$.

Figure 4.9 FESEM image of La$_{0.95}$Sr$_{0.05}$CoO$_3$.
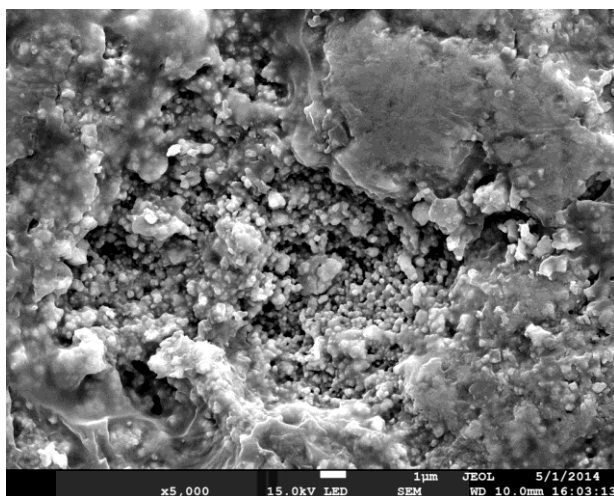
Figure 4.10 FESEM image of $La_{0.9}Sr_{0.1}CoO_3$.
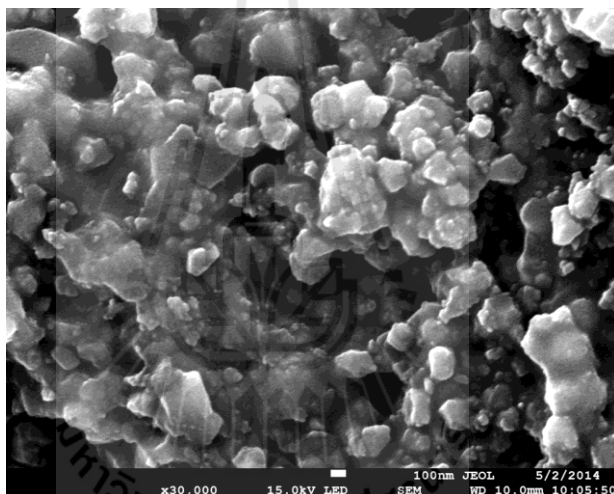
Figure 4.11 FESEM image of $La_{0.8}Sr_{0.2}CoO_3$.
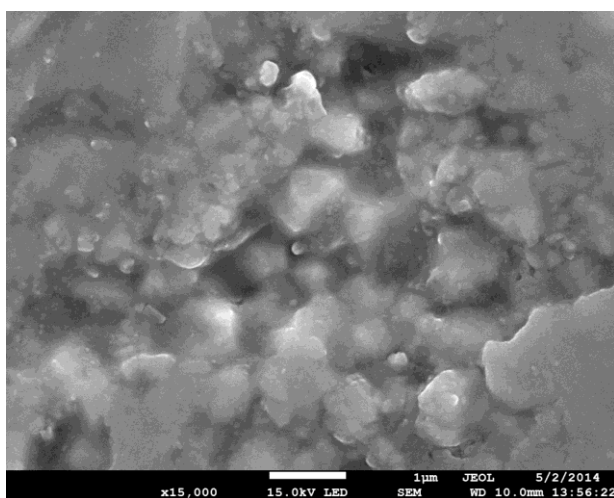
Figure 4.12 FESEM image of $LaCo_{0.98}Mg_{0.02}O_3$.
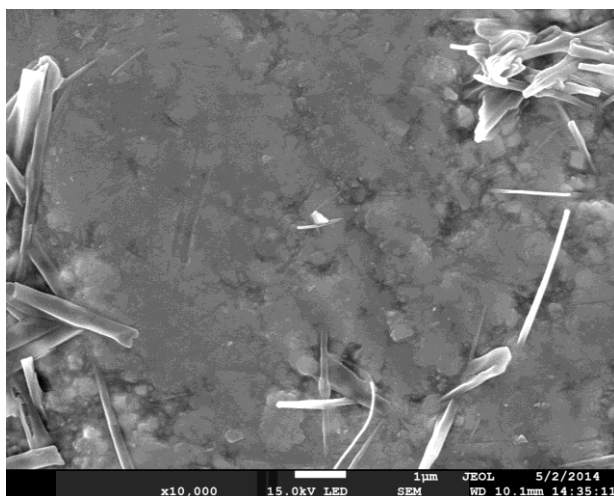
Figure 4.13 FESEM image of $LaCo_{0.95}Mg_{0.05}O_3$.
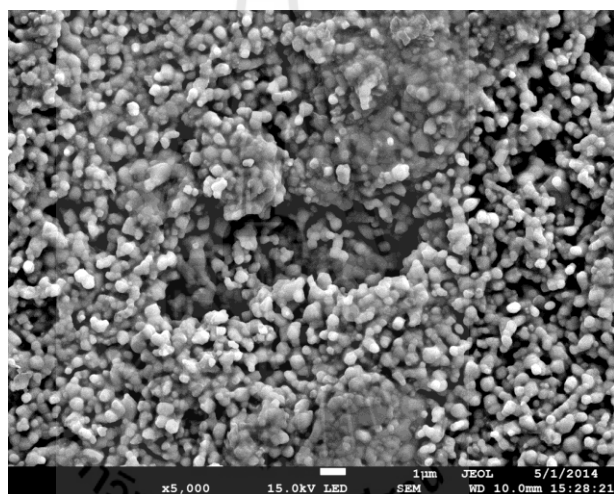
Figure 4.14 FESEM image of $LaCo_{0.9}Mg_{0.1}O_3$.
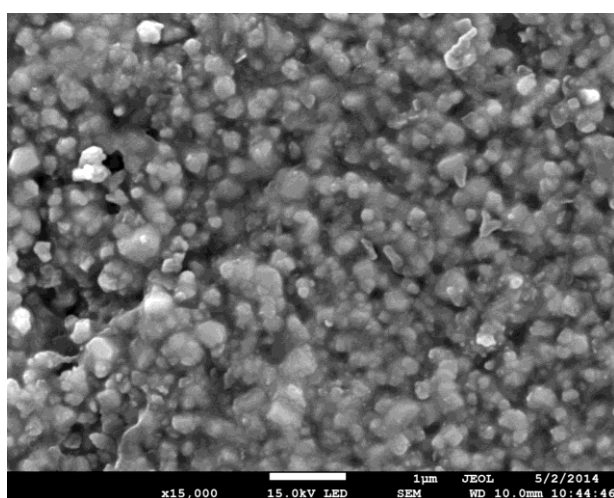
Figure 4.15 FESEM image of $LaCo_{0.8}Mg_{0.2}O_3$.
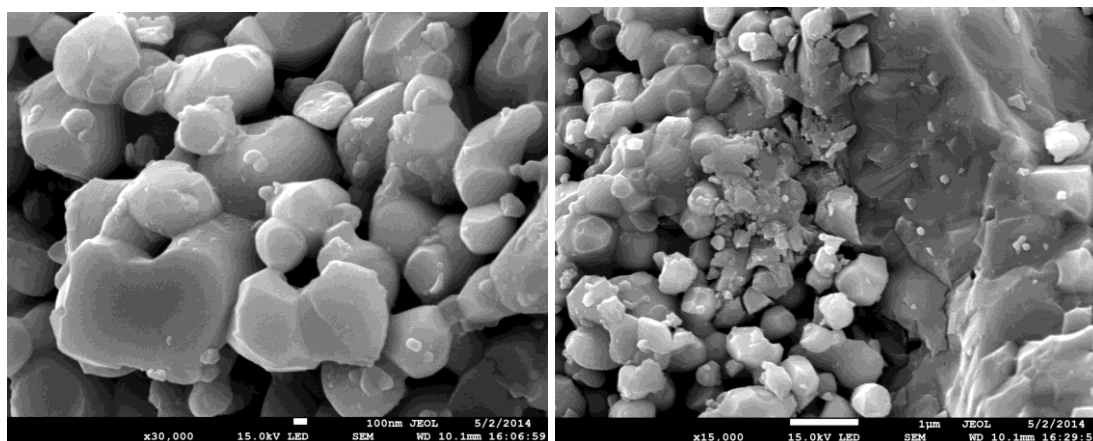
Figure 4.16 FESEM image of $La_{0.975}Sr_{0.025}Co_{0.975}Mg_{0.025}O_3$.
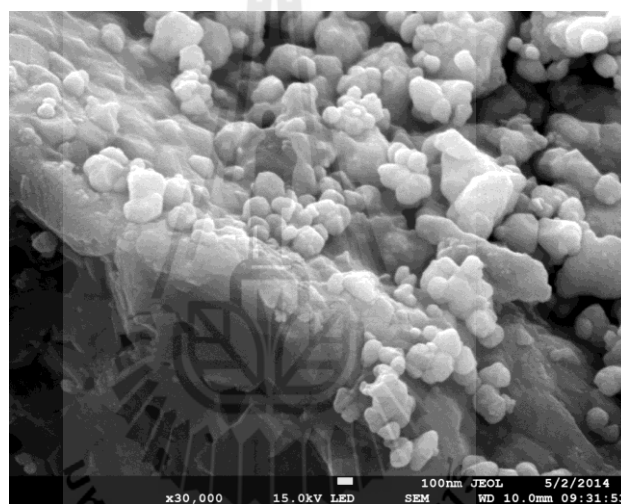
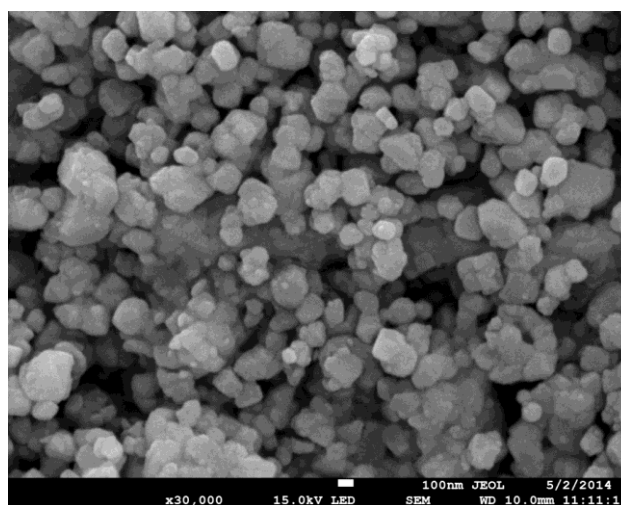**Figure 4.17** FESEM image of $La_{0.95}Sr_{0.05}Co_{0.95}Mg_{0.05}O_3$.

Figure 4.18 FESEM image of $La_{0.9}Sr_{0.1}Co_{0.9}Mg_{0.1}O_3$.

The compositions of all cations including La, Co, Sr, and Mg were confirmed by EDS technique as shown in Table 4.2.

Table 4.2 Cationic compositions of Sr and Mg doped-$LaCoO_3$ compounds.

Samples	Cationic compositions (mol)			
	La	Sr	Co	Mg
$LaCoO_3$	0.98	-	0.98	-
$La_{0.98}Sr_{0.02}CoO_3$	0.98	0.02	0.96	-
$La_{0.95}Sr_{0.05}CoO_3$	0.95	0.05	0.98	-
$La_{0.9}Sr_{0.1}CoO_3$	0.96	0.10	1.00	-
$La_{0.8}Sr_{0.2}CoO_3$	0.83	0.24	1.00	-
$LaCo_{0.98}Mg_{0.02}O_3$	1.00	-	0.91	0.02
$LaCo_{0.95}Mg_{0.05}O_3$	1.00	-	0.90	0.05
$LaCo_{0.9}Mg_{0.1}O_3$	1.00	-	0.87	0.11
$LaCo_{0.8}Mg_{0.2}O_3$	1.00	-	0.78	0.23
$La_{0.975}Sr_{0.025}Co_{0.0975}Mg_{0.025}O_3$	0.975	0.0185	0.931	0.029
$La_{0.95}Sr_{0.05}Co_{0.95}Mg_{0.05}O_3$	0.95	0.039	0.91	0.082
$La_{0.9}Sr_{0.1}Co_{0.9}Mg_{0.1}O_3$	0.90	0.13	0.90	0.12

4.3 Thermoelectric properties

4.3.1 Electrical resistivity

The evolution of electrical resistivity of the samples at room temperature with doping is shown in Figure 4.19. Both single and double substitutions of Sr and Mg decrease the electrical resistivity of $LaCoO_3$. The replacement of La^{3+} by Sr^{2+} and Co^{3+} by Mg^{2+} are compensated either by the oxidation of Co^{3+} to Co^{4+} which creates

holes, or by the introduction of oxygen vacancies (Mineshige *et al*., 1999). In general, a higher level of dopant results in lower electrical resistivity because of the higher carrier concentration as $1/\rho = ne\mu$ when n is carrier concentration, e is electric charge, and μ is carrier mobility (Snyder and Toberer, 2008). However, μ is also affected by the substitutions. Generally, Co^{4+} generated by substitutions of lower heterovalent cations enhances the Co-O bonding, and thus broadens the bandwidth to improve electron conduction (Ramadass *et al*., 1979). Therefore, substitution of Sr and Mg should result in decreased resistivity as both n and μ are increased. However, in the case of Mg substitution, the decrease of electrical resistivity is limited and the value increases when Mg content exceeds 10%. This can be explained when the electron transfer of the $LaCoO_3$ perovskite which occurs in the Co-O network of CoO_6 octahedra is taken into account. As substituted Mg locates in the said network, it may
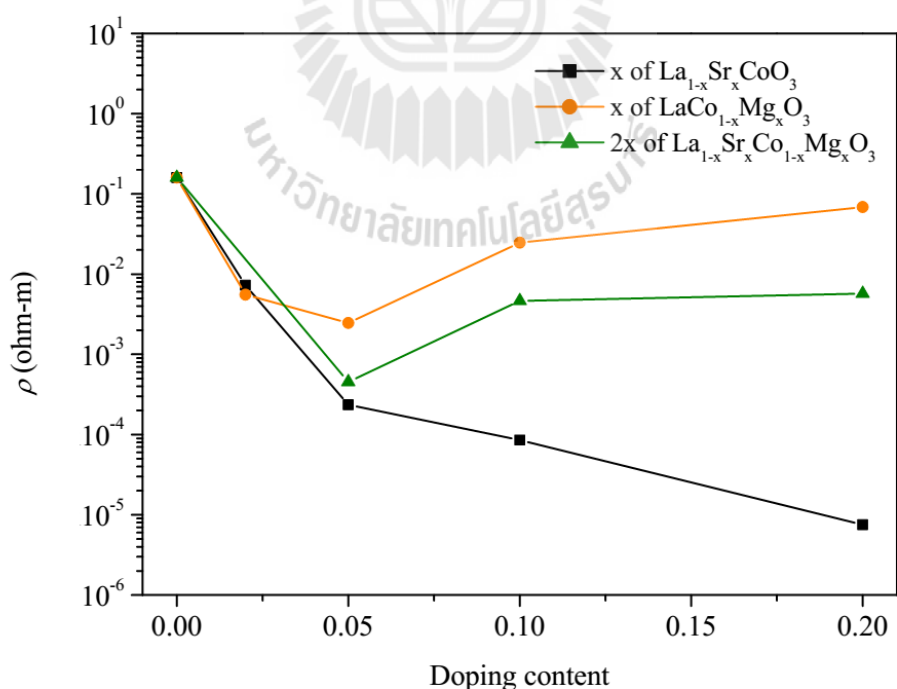

Figure 4.19 Evolution of the room-temperature electrical resistivity as a function of doping content.

block this pathway and results in decreased μ. This explanation is reasonable since there are only localized electrons in Mg^{2+}. The observed decrease of resistivity in the Mg-substituted samples is, therefore, a result of the competing mechanisms; an increase of n, an increase of μ through Co^{4+} formation, and a decrease of μ through blockage of Co-O network. In the case of Sr doping, Sr locates at the La site and does not disrupt Co-O network. Hence it should not directly affect carrier mobility in the same manner. In fact, a detailed study on Sr-substituted $LaCoO_3$ has shown that the Sr substitution increases n and μ, both of which contribute to reduce electrical resistivity (Iwasaki *et al*., 2008). The resistivity of the double-substituted samples is in between those of the Sr- doped and Mg- doped samples.

4.3.2 Seebeck coefficient

The Seebeck coefficients (S) of all samples are shown as Figure 4.20. All substituted-$LaCoO_3$ samples show positive S indicating that the main charge carriers
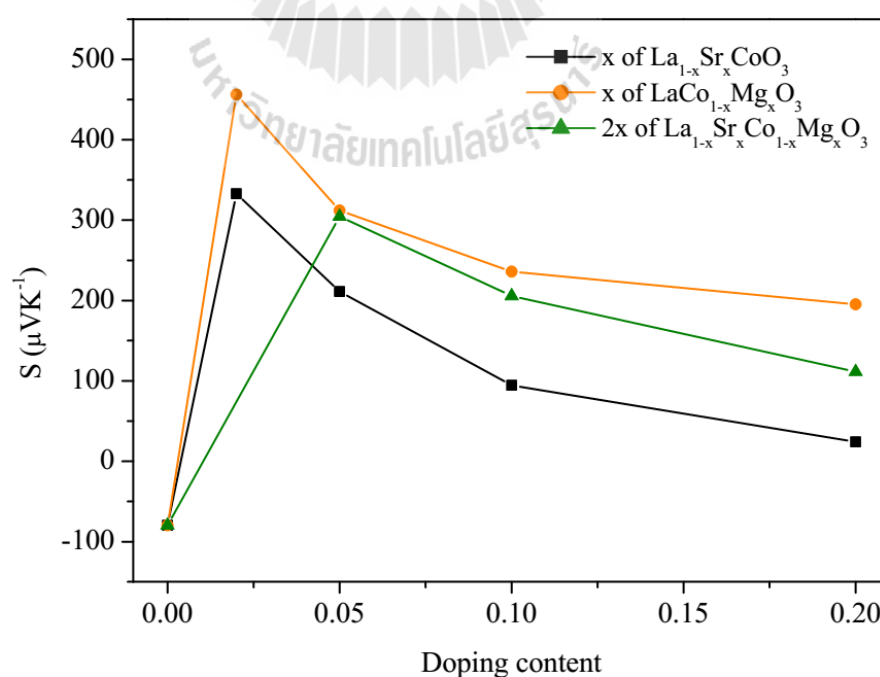

Figure 4.20 Plot of Seebeck coefficients as a function of doping content.

are holes. However, it is interesting to note that S is negative in the case of $LaCoO_3$. This effect is also reported in some other works (Iwasaki *et al*., 2008; Sehlin *et al*., 1995; Ohtani *et al*., 2000). The sign of S can be varied from negative to positive and an oxygen vacancy is assumed to be the reason (Vulchev *et al*., 2012; Berggold *et al*., 2005). The Mg substitution effectively enhances the Seebeck coefficient. The values of $LaCo_{1-y}Mg_yO_3$ with $x = 0.05$ and 0.1 prepared in this work are 312 and 236 μVK^{-1}, respectively, which are higher than 190 and 230 μVK^{-1} of those prepared by Ramadass *et al*. (1979). Nonetheless, the S of the x = 0.05 sample is lower than 400 μVK^{-1} reported by Hejtmánek *et al*. (2008).

When the samples with same doping content are compared, Mg doping has significantly larger effects in improving S than Sr doping and the Seebeck coefficients of co-doped samples are in between those of singly doped ones. Koshibe *et al*. (2000) proposed that the characteristic spin degeneracy and strong correlation of 3*d* electrons in cobalt oxides cause the large Seebeck coefficient. In the case of cobalt oxides, the Heikes formula has been used to describe the Seebeck effect; $S = -k_B/e[\ln(g_3/g_4)(x/1-x)]$ where g_3 and g_4 are the numbers of spin states for Co^{3+} and Co^{4+}, respectively, and x is the concentration of Co^{4+}. Hund's rule coupling, crystal field splitting energy (10Dq), and temperature are parameters that determine g_3 and g_4. The ratios of g_3/g_4 and x/1-x influence not only the magnitude but also the sign of S (Koshibae *et al*., 2000). In this work, the increase in the doping content leads to the decrease of the Seebeck coefficient for all cation-substituted series, which can be explained by this equation. Although the p-type substitution of $LaCoO_3$ plays an important role in decreasing electrical resistivity, it is always accompanied by the reduction of Seebeck coefficient which indicates that these two parameters are strongly correlated (Ohtaki

et al., 2011). Substitutions with other cations, i.e., Sr (Iwasaki *et al.*, 2008; Mandal *et al.*, 2005; Zhou *et al.*, 2006; Zhou *et al.*, 2008a; Zhou *et al.*, 2008b), Ba (Mandal *et al.*, 2004; Hejtmánek *et al.*, 2004), Ca (Weidenkaff *et al.*, 2008), and Ni (Kozula *et al.*, 2012; Robert *et al.*, 2006; Robert *et al.*, 2007; Vulchev *et al.*, 2012; Li and Li, 2011; Robert *et al.*, 2008), also increase electrical conductivity and decrease Seebeck coefficient. In contrast, the Mg substitution seems to have less effect in decreasing Seebeck coefficient.

4.3.3 Thermal conductivity

Thermal conductivity is plotted with doping content as shown in Figure 4.21. Total thermal conductivity (κ_T) consists of the electronic part (κ_E) and the lattice part (κ_L). Electronic thermal conductivity, which is related to electrical resistivity
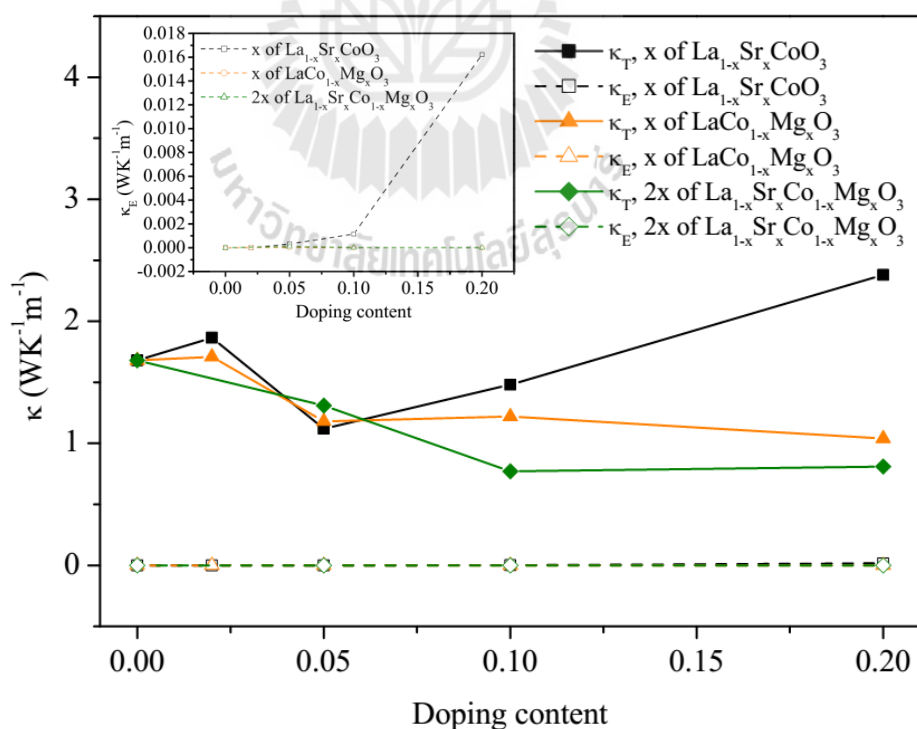

Figure 4.21 Plot of total thermal conductivity (solid line) and electronic thermal conductivity (dash line and inset) as a function of doping content.

through the Wiedemann–Franz law, ($\kappa_E = 1/\rho(LT)$, where L is the Lorenze factor), is plotted by the dash line. Lattice thermal conductivity can be calculated by subtracting the electronic part from total thermal conductivity. It is clearly seen that, in all cases, lattice thermal conductivity has more contribution to total thermal conductivity. In general, cation substitutions that create disorder in the solid structure suppress heat transfer so that the thermal conductivity is reduced. In our experiments, doping with Mg is more effective on reducing thermal conductivity than with Sr. Moreover, the decrease of thermal conductivity is more pronounced with the double substitutions, which is because they introduce more cation disordering. Note that the thermal conductivity of almost all samples are less than 2 $WK^{-1}m^{-1}$ which is considered to be the minimum value for good thermoelectric properties (Tritt and Subramanian, 2006).

4.3.4 The figure of merit ZT

Power factors, $(1/\rho)S^2$, of all samples are shown in Figure 4.22. The highest value of 0.02048 $WK^{-2}m^{-1}$ is achieved in $La_{0.975}Sr_{0.025}Co_{0.0975}Mg_{0.025}O_3$. In this sample, the Sr substitution plays an important role in increasing electrical conductivity, while the Mg substitution helps in maintaining the high Seebeck coefficient. However, when the thermal conductivity is taken into account, $La_{0.975}Sr_{0.025}Co_{0.0975}Mg_{0.025}O_3$ has a slightly lower ZT compared with that of $La_{0.95}Sr_{0.05}CoO_3$ owing to the higher thermal conductivity (Figure 4.23). $La_{0.95}Sr_{0.05}CoO_3$ prepared in this work gives a ZT of 0.052 which is slightly higher than 0.033 reported by Zhang *et al*. (2006). When the three key parameters are compared between them, our sample has less electrical resistivity, lower Seebeck coefficient and similar thermal conductivity, which result in the better ZT. In addition, a ZT of 0.021 for $La_{0.9}Sr_{0.1}CoO_3$ in this work is rather different from 0.046 reported

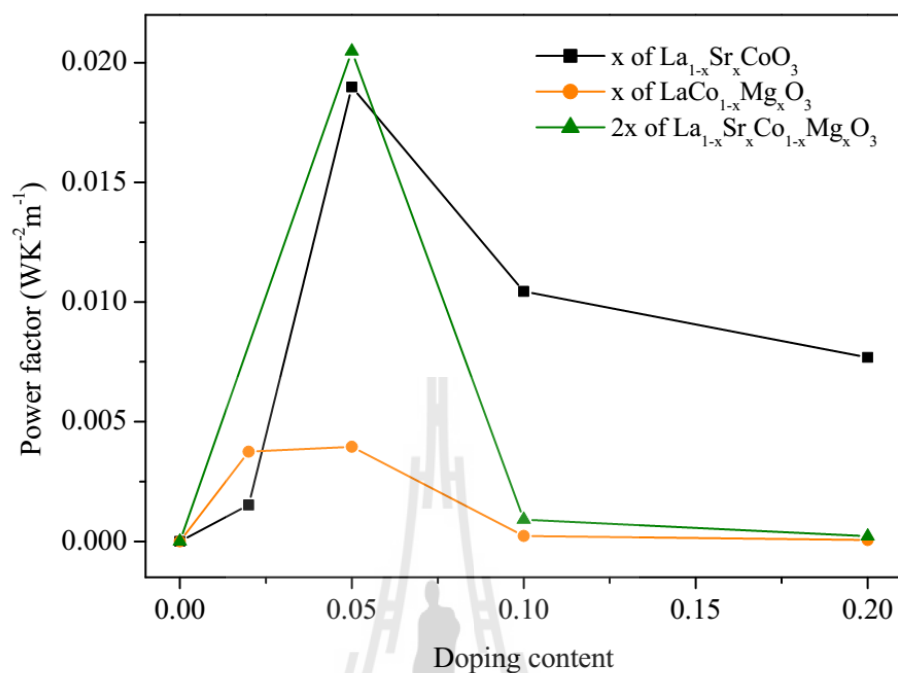by Zhou *et al*. (2008a). The reason behind these differences is unclear.

Figure 4.22 Plot of power factors as a function of doping content.
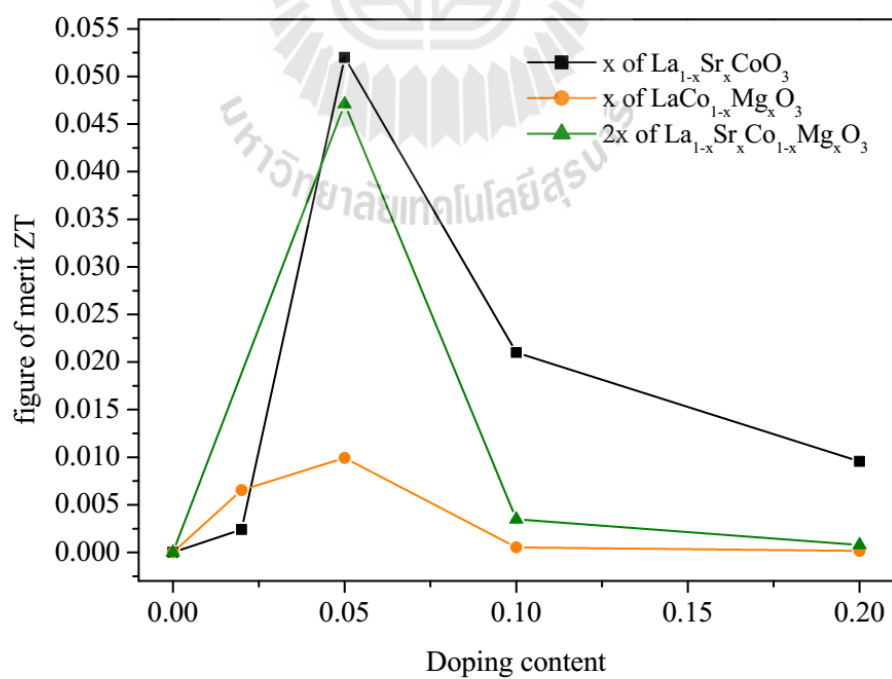

Figure 4.23 Plot of figure of merit ZT as a function of doping content at room temperature.

Some factors such as grain size, porosity, or grain boundary might have some effects and should be considered (Zhang *et al*., 2006). The density of all samples prepared in this work is approximately 80% of the theoretical density.

Although ZT values obtained here are still quite low compared with some other values reported on $LaCoO_3$ related samples such as 0.16 for $LaCo_{0.98}Ni_{0.01}Fe_{0.01}O_3$ (Vulchev *et al*., 2012), it is shown that co-substitutions in different sites can be a promising way to improve thermoelectric properties for a further development in related materials.

4.4 References

Berggold, K., Kriener, M., Zobel, C., Reichl, A., Reuther, M., Müller, R., Freimuth, A., and Lorenz, T. (2005). Thermal conductivity, thermopower, and figure of merit of $La_{1-x}Sr_xCoO_3$. **Phys. Rev. B.** 72: 155116.

Cannas, C., Musinu, A., Peddis, D., and Piccaluga, G. (2006). Synthesis and characterization of $CoFe_2O_4$ nanoparticles dispersed in a silica matrix by a sol-gel autocombustion method. **Chem. Mater.** 18: 3835-3842.

Couzi, M. and Huong, P. V. (1974). Spectres infrarouge et raman des pérovskites. **Ann. Chim.** 9: 19.

Hejtmánek, J., Jirák, Z., Knižek, K., Maryško, K., Veverka, M., and Fujishiro, H. (2004). Magnetism, structure and transport of $Y_{1-x}Ca_xCoO_3$ and $La_{1-x}Ba_xCoO_3$. **J. Magn. Magn. Mater.** 272-276: e283-e284.

Hejtmánek, J., Jirák, Z., Knížek, K., Maryško, M., Veverka, M., and Autret, C. (2008). Valence and spin states in perovskites $LaCo_{0.95}M_{0.05}O_3$ (M = Mg, Ga, Ti). **J. Magn. Magn. Mater.** 320: e92-e95.

Iwasaki, K., Ito, T., Nagasaki, T., Arita, Y., Yoshino, M., and Matsui, T. (2008). Thermoelectric properties of polycrystalline $La_{1-x}Sr_xCoO_3$. **J. Solid State Chem.** 181: 3145-3150.

Johnsson, M., and Lemmens, P. (2007). Crystallography and chemistry of perovskites. In H. Kronmüller and S. Parkin (eds.). **Handbook of magnetism and advanced magnetic materials, volume 4: Novel materials** (pp. 1-11). New York: John Wiley & Sons Inc.

Koshibae, W., Tsutsui, K., and Maekawa, S. (2000). Thermopower in cobalt oxides, **Phys. Rev. B.** 62: 6869-6872.

Kozuka, H., Ohbayashi, K., and Koumoto, K. (2012). $LaCo_{1-x}Ni_xO_3$ with improved electrical conductivity. **Inorg. Chem.** 51: 9259-9264.

Kriener, M., Zobel, C., Reichl, A., Baier, J., Cwik, M., Berggold, K., Kierspel, H., Zabara, O., Freimuth, A., and Lorenz, T. (2004). Structure, magnetization, and resistivity of $La_{1-x}M_xCoO_3$ (M = Ca, Sr, and Ba). **Phys. Rev. B.** 69: 094417.

Li, J., Smith, A. E., Kwong, K-S., Powell, C., Sleight, A. W., and Subramanian, M. A. (2010). Lattice crossover and mixed valency in the $LaCo_{1-x}Rh_xO_3$ solid solution. **J. Solid State Chem.** 183: 1388-1393.

Li, F., and Li, J-F. (2011). Effect of Ni substitution on electrical and thermoelectric properties of $LaCoO_3$ ceramics. **Ceram. Int.** 37: 105-110.

Livage, J., Henry, M., and Sanchez, C. (1988). Sol-gel chemistry of transition metal oxides. **Prog. Solid State Ch.** 18: 259-341.

Mandal, P., Choudhury, P., Biswas, S. K., and Ghosh, B. (2004). Transport and magnetic properties of $La_{1-x}Ba_xCoO_3$. **Phys. Rev. B.** 70: 104407-1-104407-8.

Mandal, P., Choudhury, P., and Ghosh, B. (2005). Transport studies of metallic $La_{1-x}A_xCoO_3$ (A = Sr, Ba) ferromagnet. **Physica B.** 359-361: 1363-1365.

Merino, N. A., Barbero, B. P., Grange, P., and Cadus, L. E. (2005). $La_{1-x}Ca_xCoO_3$ perovskite-type oxides: Preparation, characterization stability, and catalytic potentially for the total oxidation of propane. **J. Catal.** 231: 232-244.

Mineshige, A., Inaba, M., Yao, T., Ogumi, Z., Kikuchi, K., and Kawase, M. (1996). Crystal structure and metal-insulator transition of $La_{1-x}Sr_xCoO_3$. **J. Solid State Chem.** 121: 423-429.

Mineshige, A., Kobune, M., Fujii, S., Ogumi, Z., Inaba, M., Yao, T., and Kikuchi, K. (1999). Metal-insulator transition and crystal structure of $La_{1-x}Sr_xCoO_3$ as functions of Sr-content, temperature, and oxygen partial pressure. **J. Solid State Chem.** 142: 374-381.

Müller, U. (1993). **Inorganic structural chemistry.** New York: John Wiley & Sons Inc.

Ohtaki, M. (2011). Recent aspects of oxide thermoelectric materials for power generation from mid-to-high temperature heat source. **J. Ceram. Soc. Jpn.** 119: 770-775.

Ohtani, T., Kuroda, K., Matsugami, K., and Katoh, D. (2000). Electrical resistivity and thermopower of $(La_{1-x}Sr_x)MnO_3$ and $(La_{1-x}Sr_x)CoO_3$ at elevated temperatures. **J. Eur. Ceram. Soc.** 20: 2721-2726.

Øygarden, V., Lein, H. L., and Grande, T. (2012). Structure, thermal expansion and electrical conductivity of Nb-substituted $LaCoO_3$. **J. Solid State Chem.** 192: 246-254.

Pavia, D. L., Lampman, G. M., Kriz, G. S., and Vyvyan, J. R. (2009). **Introduction to**

spectroscopy (4th ed.). California: Brooks/Cole Cengage Learning.

Predoana, L., Malic, B., and Zaharescu, M. (2009). $LaCoO_3$ formation from precursors obtained by water-based sol–gel method with citric acid. **J. Therm. Anal. Calorim.** 98: 361-366.

Put, P. J. van der. (1998). **The inorganic chemistry of materials.** New York: Plenum Press.

Ramadass, N., Gopalakrishnan, J., and Sastri, M. V. C. (1979). Studies on magnesium- and titanium-substituted $LaCoO_3$. **J. Less-Common. Met.** 65: 129-138.

Rao, C. N. R. and Raveau, B. (1988). **Transition metal oxides: Structure, properties, and synthesis of ceramic oxides** (2nd ed.). New York: John Wiley & Sons, Inc.

Robert, R., Bocher, L., Trottmann, M., and Weidenkaff, A. (2006). Synthesis and high-temperature thermoelectric properties of Ni and Ti substituted $LaCoO_3$. **J. Solid State Chem.** 179: 3893-3899.

Robert, R., Bocher, L., Sipos, B., Döbeli, M., and Weidenkaff, A. (2007). Ni-doped cobaltates as potential materials for high temperature solar thermoelectric converters. **Prog. Solid State Ch.** 35: 447-455.

Robert, R., Aguirre, M. H., Bocher, L., Trottmann, M., Heiroth, S., Lippert, T., Döbeli, M., and Weidenkaff, A. (2008). Thermoelectric properties of $LaCo_{1-x}Ni_xO_3$ polycrystalline samples and epitaxial thin films. **Solid State Sci.** 10: 502-507.

Sehlin, S. R., Anderson, H. U., and Sparlin, D. M. (1995). Semiempirical model for the electrical properties of $La_{1-x}Ca_xCoO_3$. **Phys. Rev. B.** 52: 11681-11689.

Shannon, R. D., and Prewitt, C. T. (1969). Effective ionic radii in oxides and fluorides. **Acta Crystallogr. B.** 25: 925.

Shannon, R. D. (1976). Revised effective ionic radii and systematic studies of interatomic distances in halides and chalcogenides. **Acta Crystallogr. A** 32: 751.

Snyder, G. J., and Toberer, E. S. (2008). Complex thermoelectric materials. **Nat. Mater.** 7: 105-114.

Tritt, T. M., and Subramanian, M. A. (2006). Thermoelectric materials, phenomena, and applications: a bird's eye view. **Mater. Res. Bull.** 31: 188-198.

Vulchev, V., Vassilev, L., Harizanova, S., Khristov, M., Zhecheva, E., and Stoyanova, R. (2012). Improving of the thermoelectric efficiency of $LaCoO_3$ by double substitution with nickel and iron. **J. Phys. Chem. C.** 116: 13507-13515.

Weidenkaff, A., Robert, R., Aguirre, M., Bocher, L., Lippert, T., and Canulescu, S. (2008). Development of thermoelectric oxides for renewable energy conversion technologies. **Renew. Energ.** 33: 342-347.

Wells, A. F. (1995). **Structural inorganic chemistry.** London: Oxford Science publications.

Worayingyong, A., Kangvansura, P., Ausadasuk, S., and Praserthdam, P. (2008). The effect of preparation: Pechini and schiff base methods, on adsorbed oxygen of $LaCoO_3$ perovskite oxidation catalysts. **Colloid. Surface. A.** 315: 217-225.

Wu, Y., Zuo, R., Zhou, Y., and Yue, Z. (2011). Sol-gel synthesis, densification, and electrical properties of $CuO\text{-}B_2O_3$ doped $Ba_{6-3x}R_{8+2x}Ti_{18}O_{54}$ (R = Nd) microwave dielectric ceramics. **J. Mater. Sci.** 46: 1932-1936.

Zhang, X., Li, X. M., Chen, T. L., and Chen, L. D. (2006). Thermoelectric and transport properties of $La_{0.95}Sr_{0.05}CoO_3$. **J. Cryst. Growth.** 286: 1-5.

Zhou, A. J., Zhu, T. J., and Zhao, X. B. (2006). Thermoelectric properties of perovskite-type oxide $La_{1-x}Sr_xCoO_3$ (x = 0, 0.1) prepared by solid state reactions. **Mater. Sci. Eng. B.** 128: 174-178.

Zhou, A. J., Zhu, T. J., Zhao, X. B., Chen, H. Y., and Müller, E. (2008a). Fabrication and thermoelectric properties of perovskite-type oxide $La_{1-x}Sr_xCoO_3$ (x = 0, 0.1). **J. Alloy. Compd.** 449: 105-108.

Zhou, A. J., Zhu, T. J., and Zhao, X. B. (2008b). Thermoelectric properties of perovskite oxides $La_{1-x}Sr_xCoO_3$ prepared by polymerlized complex method. **J. Mater. Sci.** 43: 1520-1524.

CHAPTER V

CONCLUSION

Three series of polycrystalline samples of $La_{1-x}Sr_xCoO_3$, $LaCo_{1-x}Mg_xO_3$ (x = 0, 0.02, 0.05, 0.1, 0.2), and $La_{1-x}Sr_xCo_{1-x}Mg_xO_3$ (x = 0, 0.025, 0.05, 0.1) have been successfully prepared without impurity phases by the citrate sol-gel method. The cations compositions were confirmed by EDS. Increasing the amount of dopants, Sr and Mg, causes expansions in cell parameters *a* and *c,* because bigger Sr and Mg atoms are substituted for La and Co atoms, respectively. Thermoelectric properties of all series have been examined in terms of electrical resistivity (ρ), Seebeck coefficient (S), and thermal conductivity (κ) measurements. Compared with $LaCoO_3$, resistivity is decreased after replacing La by Sr, but not by as much in the case of Mg doping because Mg may block the electron transfer pathway in the CoO_6 network. On the other hand, Mg substitution has more effect in maintaining a high Seebeck coefficient. The double substitution of Sr and Mg improves the thermoelectric properties as evidenced by the increase in the power factor. In addition, the double substitution also decreases the lattice part of thermal conductivity, which further improves their thermoelectric efficiency. Among all the double-substituted samples studied in this work, $La_{0.975}Sr_{0.025}Co_{0.0975}Mg_{0.025}O_3$ gives the best ZT of 0.047 at room temperature.

APPENDICES

APPENDIX A

CALCULATION: A SAMPLE PREPARATION

AND A SAMPLE DENSITY

A.1 Calculation of a sample preparation

Samples of $La_{1-x}Sr_xCoO_3$, $LaCo_{1-x}Mg_xO_3$ (x = 0, 0.02, 0.05, 0.1, 0.2), and $La_{1-x}Sr_xCo_{1-x}Mg_xO_3$ (x = 0, 0.025, 0.05, 0.1) were prepared by weighting starting materials in a stoichiometric ratio. The calculation procedure is as following;

Firstly, the number of mol of a sample is calculated using molecular weight (M.W.) of a sample.

mol of a sample = (gram of a sample)/(M.W. of a sample)

Secondly, a weight of each precursor is calculated using its M.W., mol of a sample (from the first step), and mol of an atom (in a formula).

weight of a precursor = (M.W. of a precursor) x (mol of a sample) x

(mol of an atom)

For example, 1 gram of $La_{0.9}Sr_{0.1}Co_{0.9}Mg_{0.1}O_3$ can be prepared by following calculations;

mol of $La_{0.9}Sr_{0.1}Co_{0.9}Mg_{0.1}O_3$ = 1 g/(237.25 g/mol)

= 0.004214963119 mol

weight of $La(NO_3)_3 \cdot 6H_2O$ = 433.01 g/mol x 0.004214963119 mol x 0.9 mol

= 1.6426 g

weight of $Co(NO_3)_2 \cdot 6H_2O$ = 291.03 g/mol x 0.004214963119 mol x 0.9 mol

= 1.1040 g

weight of $Sr(NO_3)_2$ = 211.63 g/mol x 0.004214963119 mol x 0.1 mol

= 0.0892 g

weight of $Mg(NO_3)_2 \cdot 6H_2O$ = 256.41 g/mol x 0.004214963119 mol x 0.1 mol

= 0.1081 g

Regarding the ratio of cations:citric acid (1:4), mol of a citric acid can be calculated by multiplying mol of a sample, mol of a an atom, and M.W. of a citric acid ($C_6H_8O_7 \cdot H_2O$) by 4.

weight of a citric acid for $La(NO_3)_3 \cdot 6H_2O$

= 210.14 g/mol x 0.004214963119 mol x 0.9 mol

= 0.7972 g

weight of a citric acid for $Co(NO_3)_2 \cdot 6H_2O$

= 210.14 g/mol x 0.004214963119 mol x 0.9 mol

= 0.7972 g

weight of a citric acid for $Sr(NO_3)_2$

= 210.14 g/mol x 0.004214963119 mol x 0.1 mol

= 0.0886 g

weight of a citric acid for $Mg(NO_3)_2 \cdot 6H_2O$

= 210.14 g/mol x 0.004214963119 mol x 0.1 mol

= 0.0886 g

A.2 Calculation of a sample density

In this work, a density of all samples is calculated generally as it is equal to mass divided by volume; density of a sample = mass/volume. A volume can be obtained depending on a sample's geometry. Percent of density is then reported comparing to their theoretical density. A theoretical density can be calculated from M.W. of a sample, cell volume (calculated from lattice parameters), a number of atoms per unit cell (Z), and Avogadro's number (6.023×10^{23} /mol).

$$\text{Theoretical density} = \frac{\text{Z x M.W.of a sample}}{\text{cell volume x Avogadro's number}}$$

For example, the density of $LaCoO_3$ is as

$$= \text{mass/volume}$$

$$= 0.1380 \text{ g}/0.02366 \text{ cm}^3$$

$$= 5.8319 \text{ g/cm}^3$$

The theoretical density of $LaCoO_3$ is as

$$= \frac{\text{Z x M.W.of a sample}}{\text{cell volume x Avogadro's number}}$$

$$= \frac{6 \times 245.84 \text{ g.mol}^{-1}}{387.85 \text{ cm}^3 \times 6.023 \times 10^{23} \text{ mol}^{-1}}$$

$$= 6.3142 \text{ g/cm}^3$$

So, the sample density percentage of $LaCoO_3$ is as

$$= \frac{\text{a sample density}}{\text{a theoretical density}} \times 100$$

$$= \frac{5.8319 \text{ g.}cm^3}{6.3142 \text{ g.}cm^3} \times 100$$

$$= 92.36\%$$

APPENDIX B

THESIS OUTPUT

Jiamprasertboon, A., Okamoto, Y., Hiroi, Z., and Siritanon, T. (2014). Thermoelectric properties of Sr and Mg double-substituted $LaCoO_3$ at room temperature. **Ceram. Int.** 40: 12729-12735.

CURRICULUM VITAE

Name   Miss Arreerat jiamprasertboon

Date of Birth July 3rd, 1988, Ubon Ratchathani, Thailand

Address   250 Village no.2, Khulu Sub-District, Trakan Phut Phon District, Ubon Ratchathani Province, Thailand, 34130

Education

2007-2010   B.Sc. First Class Honors (Chemistry), Khon Kaen University, Thailand with scholarship from Thai government, "Development and Promotion of Science and Technology Talent Project, DPST"

2011-2013   Student at department of chemistry, Suranaree University of Technology, Thailand with scholarship from Thai government, "Development and Promotion of Science and Technology Talent Project, DPST"

Publication

Jiamprasertboon, A., Okamoto, Y., Hiroi, Z., and Siritanon, T. (2014). Thermoelectric properties of Sr and Mg double-substituted LaCoO$_3$ at room temperature. **Ceram. Int.** 40: 12729-12735.